CHAPTER 58
STEAM TURBINES

William G. Steltz
Turboflow International Inc.
Orlando, Florida

58.1 HISTORICAL BACKGROUND

The process of generating power depends on several energy-conversion processes, starting with the chemical energy in fossil fuels or the nuclear energy within the atom. This energy is converted to thermal energy, which is then transferred to the working fluid, in our case, steam. This thermal energy is converted to mechanical energy with the help of a high-speed turbine rotor and a final conversion to electrical energy is made by means of an electrical generator in the electrical power-generation application. The presentation in this section focuses on the electrical power application, but is also relevant to other applications, such as ship propulsion.

Throughout the world, the power-generation industry relies primarily on the steam turbine for the production of electrical energy. In the United States, approximately 77% of installed power-generating capacity is steam turbine-driven. Of the remaining 23%, hydroelectric installations contribute 13%, gas turbines account for 9%, and the remaining 1% is split among geothermal, diesel, and solar power sources. In effect, over 99% of electric power generated in the United States is developed by turbomachinery of one design or another, with steam turbines carrying by far the greatest share of the burden.

Steam turbines have had a long and eventful life since their initial practical development in the late 19th century due primarily to efforts led by C. A. Parsons and G. deLaval. Significant developments came quite rapidly in those early days in the fields of ship propulsion and later in the power-generation industry. Steam conditions at the throttle progressively climbed, contributing to increases in power production and thermal efficiency. The recent advent of nuclear energy as a heat source for power production had an opposite effect in the late 1950s. Steam conditions tumbled to accommodate reactor designs, and unit heat rates underwent a step change increase. By this time, fossil unit throttle steam conditions had essentially settled out at 2400 psi and 1000°F with single reheat to 1000°F. Further advances in steam powerplants were achieved by the use of once-through boilers delivering supercritical pressure steam at 3500–4500 psi. A unique steam plant utilizing advanced steam con-

This chapter was previously published in J. A. Schetz and A. E. Fuhs (eds.), *Handbook of Fluid Dynamics and Fluid Machinery,* Vol. 3, *Applications of Fluid Dynamics,* New York, Wiley, 1996, Chapter 27.

Mechanical Engineers' Handbook, 2nd ed., Edited by Myer Kutz.
ISBN 0-471-13007-9

ditions is Eddystone No. 1, designed to deliver steam at 5000 psi and 1200°F to the throttle, with reheat to 1050°F and second reheat also to 1050°F.

Unit sizes increased rapidly in the period from 1950 to 1970; the maximum unit size increased from 200 mW to 1200 mW (a sixfold increase) in this span of 20 years. In the 1970s, unit sizes stabilized, with new units generally rated at substantially less than the maximum size. At the present time, however, the expected size of new units is considerably less, appearing to be in the range of 350–500 mW.

In terms of heat rate (or thermal efficiency), the changes have not been so dramatic. A general trend showing the reduction of power station heat rate over an 80-year period is presented in Fig. 58.1. The advent of regenerative feedwater heating in the 1920s brought about a step change reduction in heat rate. A further reduction was brought about by the introduction of steam reheating. Gradual improvements continued in steam systems and were recently supplemented by the technology of the combined cycle, the gas turbine/steam turbine system (see Fig. 58.2). In the same period of time that unit sizes changed by a factor of six (1950 to 1970), heat rate diminished by less than 20%, a change that includes the combined cycle. In reality, the improvement is even less, as environmental regulations and the energy required to satisfy them can consume up to 6% or so of a unit's generated power.

The rate of improvement of turbine cycle heat rate is obviously decreasing. Powerplant and machinery designers are working hard to achieve small improvements both in new designs and in retrofit and repowering programs tailored to existing units. Considering the worth of energy, what, then, are our options leading to thermal performance improvements and the management of our energy and financial resources? Exotic energy-conversion processes are a possibility: MHD, solar

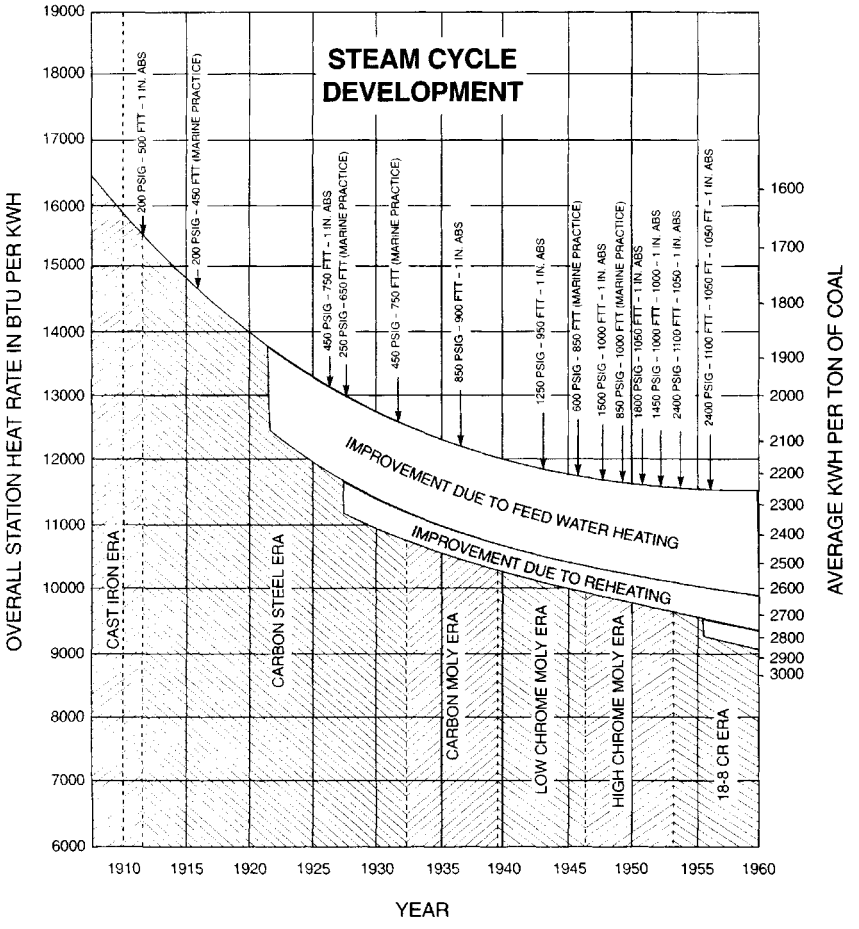

Fig. 58.1 Steam cycle development.

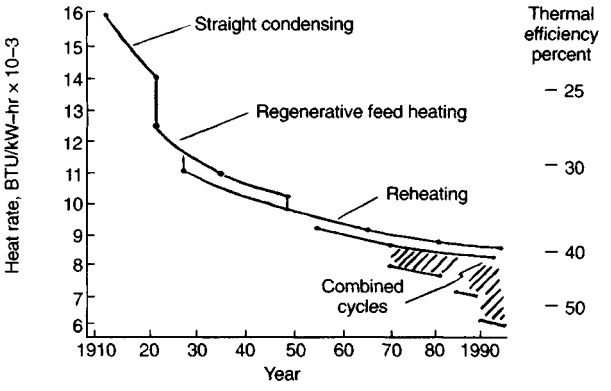

Fig. 58.2 Fossil-fueled unit heat rate as a function of time.

power, the breeder reactor, and fusion are some of the longer-range possibilities. A more near-term possibility is through the improvement (increase) of steam conditions. The effect of improved steam conditions on turbine cycle heat rate is shown in Fig. 58.3, where heat rate is plotted as a function of throttle pressure with parameters of steam temperature level. The plus mark indicates the placement of the Eddystone unit previously mentioned.

58.2 THE HEAT ENGINE AND ENERGY CONVERSION PROCESSES

The mechanism for conversion of thermal energy is the *heat engine,* a thermodynamic concept, defined and sketched out by Carnot and applied by many, the power generation industry in particular. The heat engine is a device that accepts thermal energy (heat) as input and converts this energy to useful work. In the process, it rejects a portion of this supplied heat as unusable by the work production process. The efficiency of the ideal conversion process is known as the *Carnot efficiency.* It serves as a guide to the practitioner and as a limit for which no practical process can exceed. The Carnot efficiency is defined in terms of the absolute temperatures of the heat source T_{hot} and the heat sink T_{cold} as follows:

$$\text{Carnot efficiency} = \frac{T_{hot} - T_{cold}}{T_{hot}} \tag{58.1}$$

Consider Fig. 58.4, which depicts a heat engine in fundamental terms consisting of a quantity of heat supplied, heat added, a quantity of heat rejected, heat rejected. and an amount of useful work done, work done. The *thermal efficiency* of this basic engine can be defined as

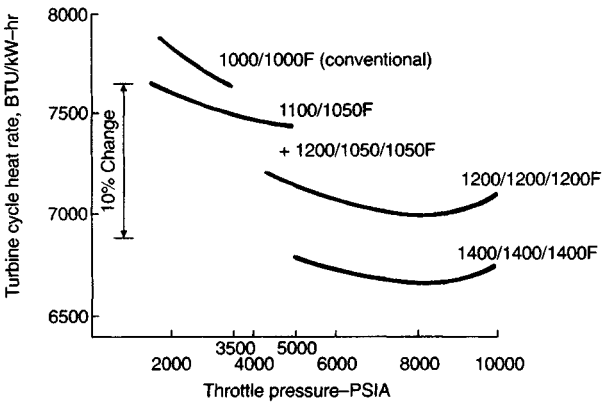

Fig. 58.3 Comparison of turbine cycle heat rate as a function of steam conditions.

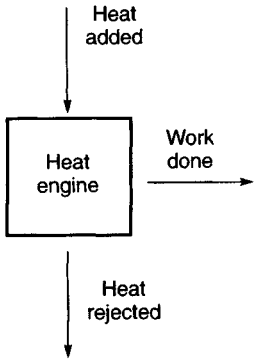

Fig. 58.4 The basic heat engine.

$$\text{efficiency} = \frac{\text{work done}}{\text{heat added}} \tag{58.2}$$

This thermal efficiency is fundamental to any heat engine and is, in effect, a measure of the heat rate of any turbine-generator unit of interest. Figure 58.5 is the same basic heat engine redefined in terms of turbine cycle terminology, that is, heat added is the heat input to the steam generator, heat rejected is the heat removed by the condenser, and the difference is the work done (power) produced by the turbine cycle. Figure 58.6 is a depiction of a simple turbine cycle showing the same parameters, but described in conventional terms. *Heat rate* is now defined as the quantity of heat input required to generate a unit of electrical power (kW).

$$\text{heat rate} = \frac{\text{heat added}}{\text{work done}} \tag{58.3}$$

The units of heat rate are usually in terms of Btu/kW·hr.

Further definition of the turbine cycle is presented in Fig. 58.7, which shows the simple turbine cycle with pumps and a feedwater heater included (of the open type). In this instance, two types of heat rate are identified: (1) a *gross heat rate,* in which the turbine-generator set's natural output (i.e., gross electrical power) is the denominator of the heat rate expression, and (2) a *net heat rate,* in which the gross power output has been debited by the power requirement of the boiler feed pump, resulting in a larger numeric value of heat rate. This procedure is conventional in the power-generation industry, as it accounts for the inner requirements of the cycle needed to make it operate. In other, more complex cycles, the boiler feed pump power might be supplied by a steam turbine-driven feed pump. These effects are then included in the heat balance describing the unit's performance.

The same accounting procedures are true for all cycles, regardless of their complexity. A typical 450-mW fossil unit turbine cycle heat balance is presented in Fig. 58.8. Steam conditions are 2415

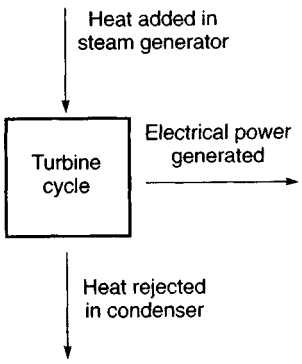

Fig. 58.5 The basic heat engine described in today's terms.

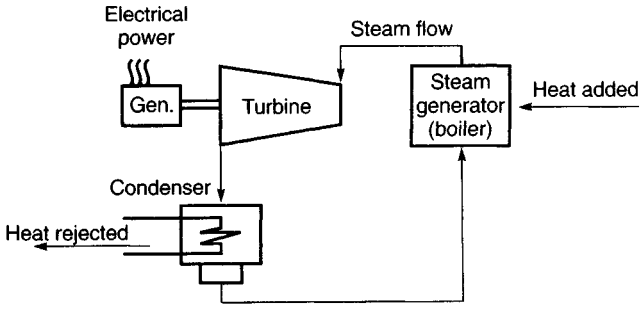

$$\text{Thermal efficiency} = \frac{\text{Electrical power}}{\text{Heat added}}$$

$$\text{Heat rate} = \frac{\text{Heat added}}{\text{Electrical power}}, \text{ BTU/kW–hr}$$

Fig. 58.6 A simple turbine cycle.

psia/1000°F/1000°F/2.5 inHga, and the cycle features seven feedwater heaters and a motor-driven boiler feed pump. Only pertinent flow and steam property parameters have been shown, in order to avoid confusion and to support the conceptual simplicity of heat rate. As shown in the two heat rate expressions, only two flow rates, four enthalpies, and two kW values are required to determine the gross and net heat rates of 8044 and 8272 Btu/kW·hr, respectively.

To supplement the fossil unit of Fig. 58.8, Fig. 58.9 presents a typical nuclear unit of 1000 mW capability. Again, only the pertinent parameters are included in this sketch for simplicity. Steam conditions at the throttle are 690 psi with ¼% moisture, and the condenser pressure is 3.0 inHga. The cycle features six feedwater heaters, a steam turbine-driven feed pump, and a moisture separator reheater (MSR). The reheater portion of the MSR takes throttle steam to heat the low-pressure (LP) flow to 473°F from 369°F (saturation at 164 psia). In this cycle, the feed pump is turbine-driven by steam taken from the MSR exit; hence, only one heat rate is shown, the net heat rate, 10,516 Btu/kW·hr. This heat rate comprises only four numbers, the throttle mass flow rate, the throttle enthalpy, the final feedwater enthalpy, and the net power output of the cycle.

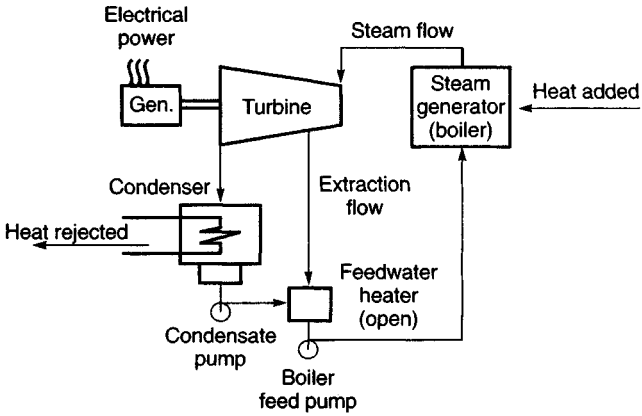

$$\text{Gross heat rate} = \frac{\text{Heat added}}{\text{Electrical power}}, \text{ BTU/kW–hr}$$

$$\text{Net heat rate} = \frac{\text{Heat added}}{\text{Electrical power–BFP power}}, \text{ BTU/kW–hr}$$

Fig. 58.7 A simple turbine cycle with an open heater and a boiler feed pump.

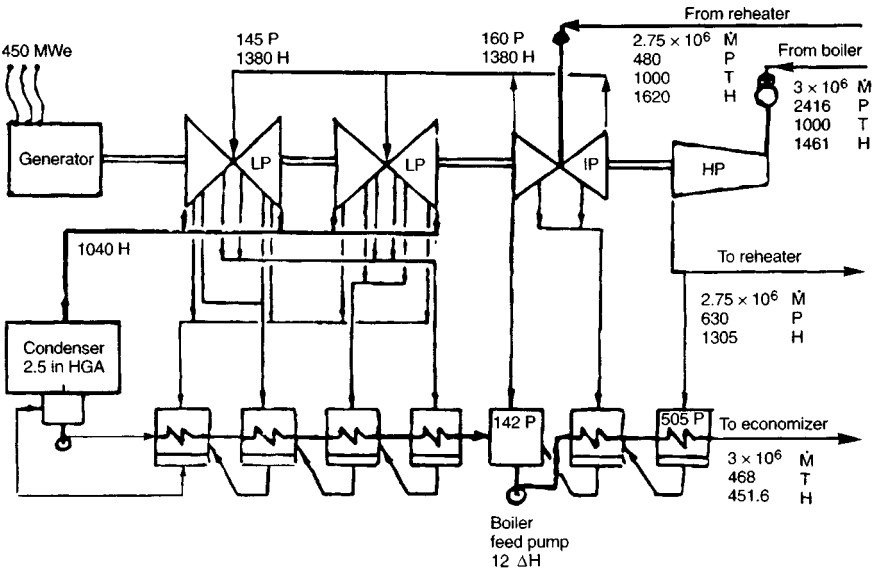

$$\text{Gross heat rate} = \frac{3{,}000{,}000\,(1461 - 451.6) + 2{,}760{,}000\,(1520 - 1305)}{450{,}000} = 8044 \text{ BTU/kW–hr}$$

$$\text{Net heat rate} = \frac{3{,}000{,}000\,(1461 - 451.6) + 2{,}760{,}000\,(1520 - 1305)}{450{,}000 - 12{,}400} = 8272 \text{ BTU/kW–hr}$$

Fig. 58.8 Typical fossil unit turbine cycle heat balance.

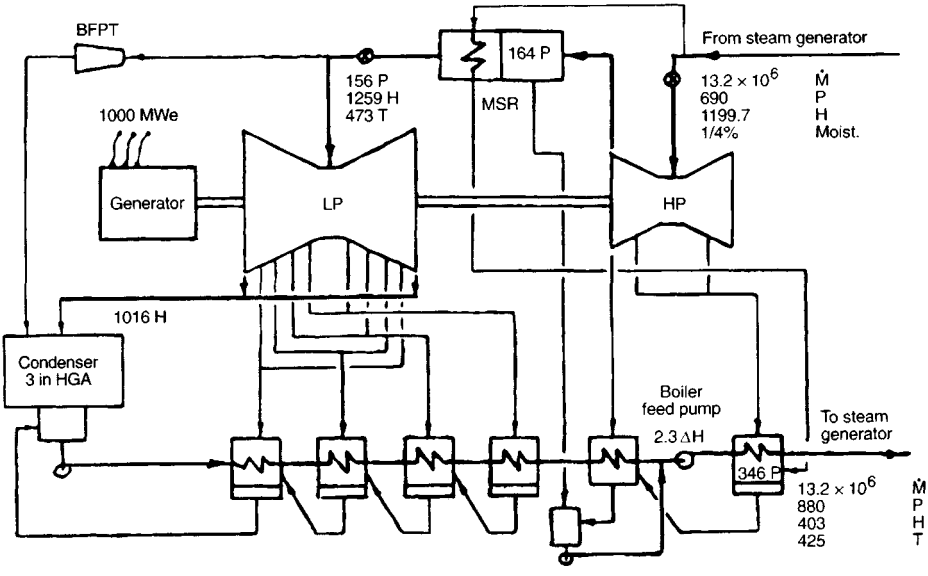

$$\text{Net heat rate} = \frac{13{,}200{,}000\,(1199.7 - 403)}{1{,}000{,}000} = 10516 \text{ BTU/kW–hr}$$

Fig. 58.9 Typical nuclear unit turbine cycle heat balance.

For comparative purposes, the expansion lines of the fossil and nuclear units of Figs. 58.8 and 58.9 have been superimposed on the *Mollier diagram* of Fig. 58.10. It is easy to see the great difference in steam conditions encompassed by the two designs and to relate the ratio of cold to hot temperatures to their Carnot efficiencies. In the terms of Carnot, the maximum fossil unit thermal efficiency would be 61% and the maximum nuclear unit thermal efficiency would be 40%. The ratio of these two Carnot efficiencies (1.53) compares somewhat favorably with the ratio of their net heat rates (1.27).

To this point, emphasis has been placed on the *conventional* steam turbine cycle, where conventional implies the central station power-generating unit whose energy source is either a fossil fuel (coal, oil, gas) or a fissionable nuclear fuel. Figure 58.2 has shown a significant improvement in heat rate attributable to *combined cycle* technology, that is, the marriage of the gas turbine used as a *topping unit* and the steam turbine used as a *bottoming unit.* The cycle efficiency benefits come from the high firing temperature level of the gas turbine, current units in service operating at 2300°F, and the utilization of its waste heat to generate steam in a heat-recovery steam generator (HRSG). Figure 58.11 is a heat balance diagram of a simplified combined cycle showing a two-pressure-level HRSG. The purpose of the two-pressure-level (or even three-pressure-level) HRSG is the minimization of the temperature differences existing between the gas turbine exhaust and the evaporating water/steam mixture. Second Law analyses (commonly termed *availability* or *exergy analyses*) result in improved cycle thermal efficiency when integrated average values of the various heat-exchanger temperature differences are small. The smaller, the better, from an efficiency viewpoint; however, the smaller the

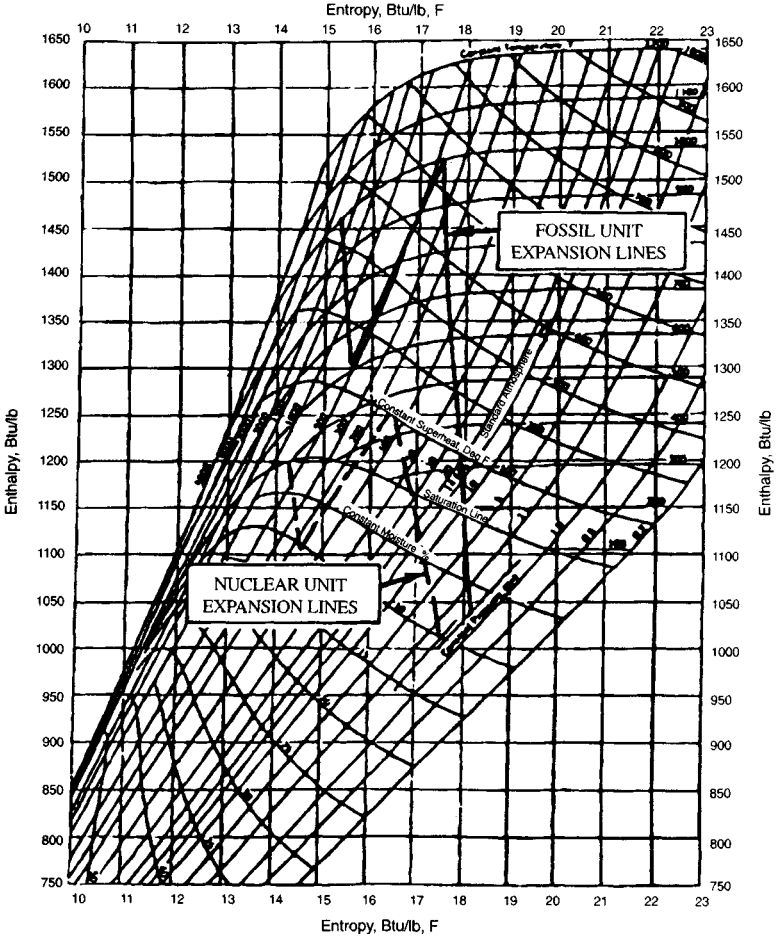

Fig. 58.10 Fossil and nuclear unit turbine expansion lines superimposed on the Mollier diagram.

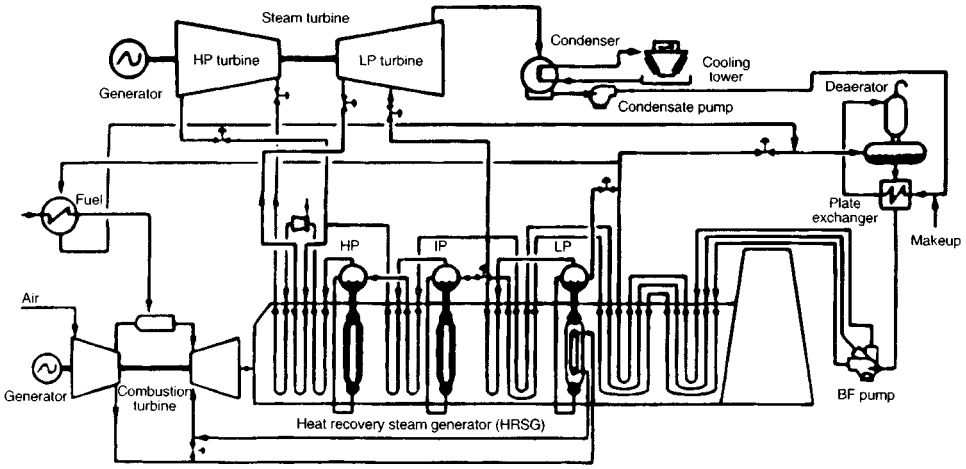

Fig. 58.11 A typical combined cycle plant schematic.

temperature difference, the larger the required physical heat transfer area. These Second Law results are then reflected by the cycle heat balance, which is basically a consequence of the First Law of thermodynamics (conservation of energy) and the conservation of mass. As implied by Fig. 58.11, a typical combined cycle schematic, the heat rate is about 6300 Btu/kW·hr, and the corresponding cycle thermal efficiency is about 54%, about ten points better than a conventional standalone fossil steam turbine cycle.

A major concept of the Federal Energy Policy of 1992 is the attainment of an Advanced Turbine System (ATS) thermal efficiency of 60% by the year 2000. Needless to say, significant innovative approaches will be required in order to achieve this ambitious level. The several approaches to this end include the increase of gas turbine inlet temperature and probably pressure ratio, reduction of cooling flow requirements, and generic reduction of blade path aerodynamic losses. On the steam turbine side, reduction of blade path aerodynamic losses and most likely increased inlet steam temperatures to be compatible with the gas turbine exhaust temperature are required.

A possibility that is undergoing active development is the use of an ammonia/water mixture as the working fluid of the gas turbine's bottoming cycle in place of pure water. This concept known as the *Kalina cycle*[1] promises a significant improvement to cycle thermal efficiency primarily by means of the reduction of losses in system *availability*. Physically, a practical ammonia/water system requires a number of heat exchangers, pumps and piping, and a turbine that is smaller than its steam counterpart due to the higher pressure levels that are a consequence of the ammonia/water working fluid.

58.3 SELECTED STEAM THERMODYNAMIC PROPERTIES

Steam has had a long history of research applied to the determination of its thermodynamic and transport properties. The currently accepted description of steam's thermodynamic properties is the ASME Properties of Steam publication.[2] The Mollier diagram, the plot of enthalpy versus entropy, is the single most significant and useful steam property relationship applicable to the steam turbine machinery and cycle designer/analyst (see Fig. 58.12).

There are, however, several other parameters that are just as important and that require special attention. Although not a perfect gas, steam may be treated as such, provided the appropriate perfect gas parameters are used for the conditions of interest. The cornerstone of perfect gas analysis is the requirement that $pv = RT$. For nonperfect gases, a factor Z may be defined such that $pv = RZT$ where the product RZ in effect replaces the particular gas constant R. For steam, this relationship is described in Fig. 58.13, where RZ has been divided by J, Joule's constant.

A second parameter pertaining to perfect gas analysis is the isentropic expansion exponent given in Fig. 58.14. (The definition of the exponent is given in the caption on the figure.) Note that the value of γ well represents the properties of steam for a *short* isentropic expansion. It is the author's experience that accurate results are achievable at least over a 2:1 pressure ratio using an average value of the exponent.

The first of the derived quantities relates the critical flow rate of steam[3] to the flow system's inlet pressure and enthalpy, as in Fig. 58.15. The critical (maximum) mass flow rate M, assuming an isentropic expansion process and equilibrium steam properties, is obtained by multiplying the ordinate value K by the inlet pressure p_1 in psia and the passage throat area A in square inches:

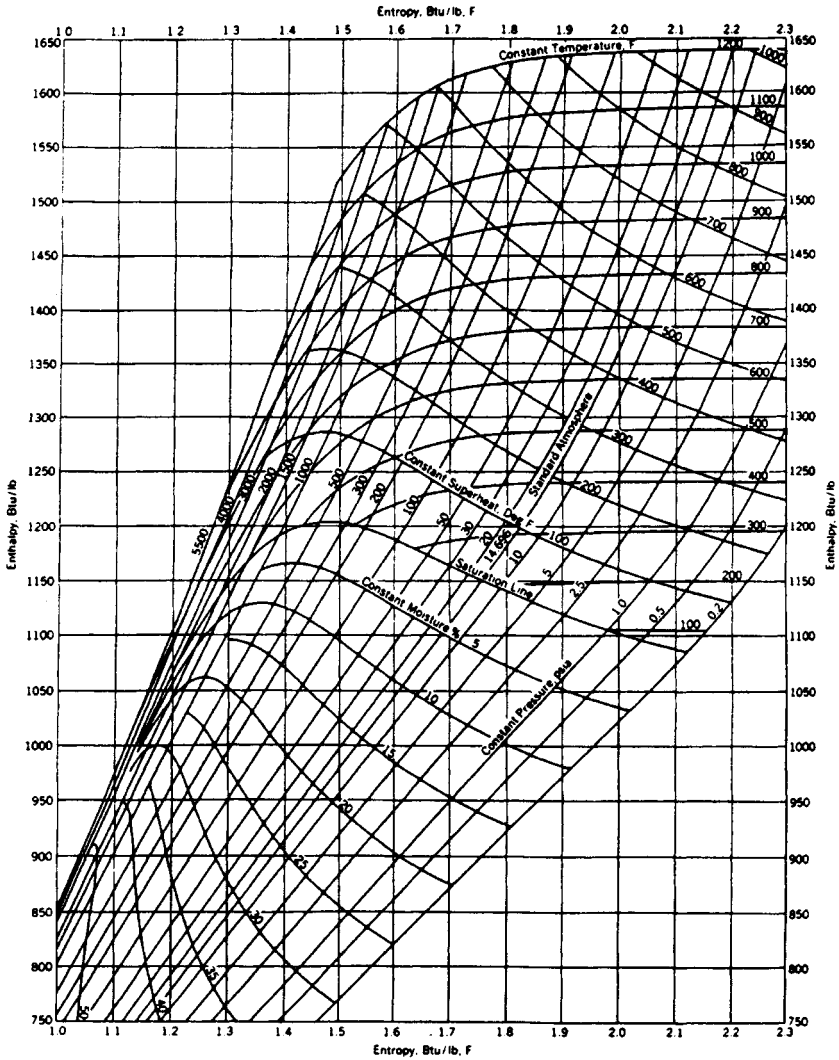

Fig. 58.12 Mollier diagram (h-s) for steam. (From Ref. 4.)

$$\dot{M}_{\text{critical}} = p_1 K A \tag{58.4}$$

The actual steam flow rate can then be determined as a function of actual operating conditions and geometry.

The corresponding choking velocity (acoustic velocity in the superheated steam region) is shown in Figs. 58.16 and 58.17 for superheated steam and wet steam, respectively. The range of Mach numbers experienced in steam turbines can be put in terms of the *wheel speed Mach number,* that is, the rotor tangential velocity divided by the local acoustic velocity. In the HP turbine, wheel speed is on the order of 600 ft/sec, while the acoustic velocity at 2000 psia and 975°F is about 2140 ft/sec; hence, the wheel speed Mach number is 0.28. For the last rotating blade of the LP turbine, its tip wheel speed could be as high as 2050 ft/sec. At a pressure level of 1.0 psia and an enthalpy of 1050 Btu/lb, the choking velocity is 1275 ft/sec; hence, the wheel speed Mach number is 1.60. As Mach numbers relative to either the stationary or rotating blading are approximately comparable, the steam turbine designer must negotiate flow regimes from incompressible flow, low subsonic Mach number of 0.3, to supersonic Mach numbers on the order of 1.6.

Another quite useful characteristic of steam is the product of pressure and specific volume plotted versus enthalpy in Figs. 58.18 and 58.19 for low-temperature/wet steam and superheated steam,

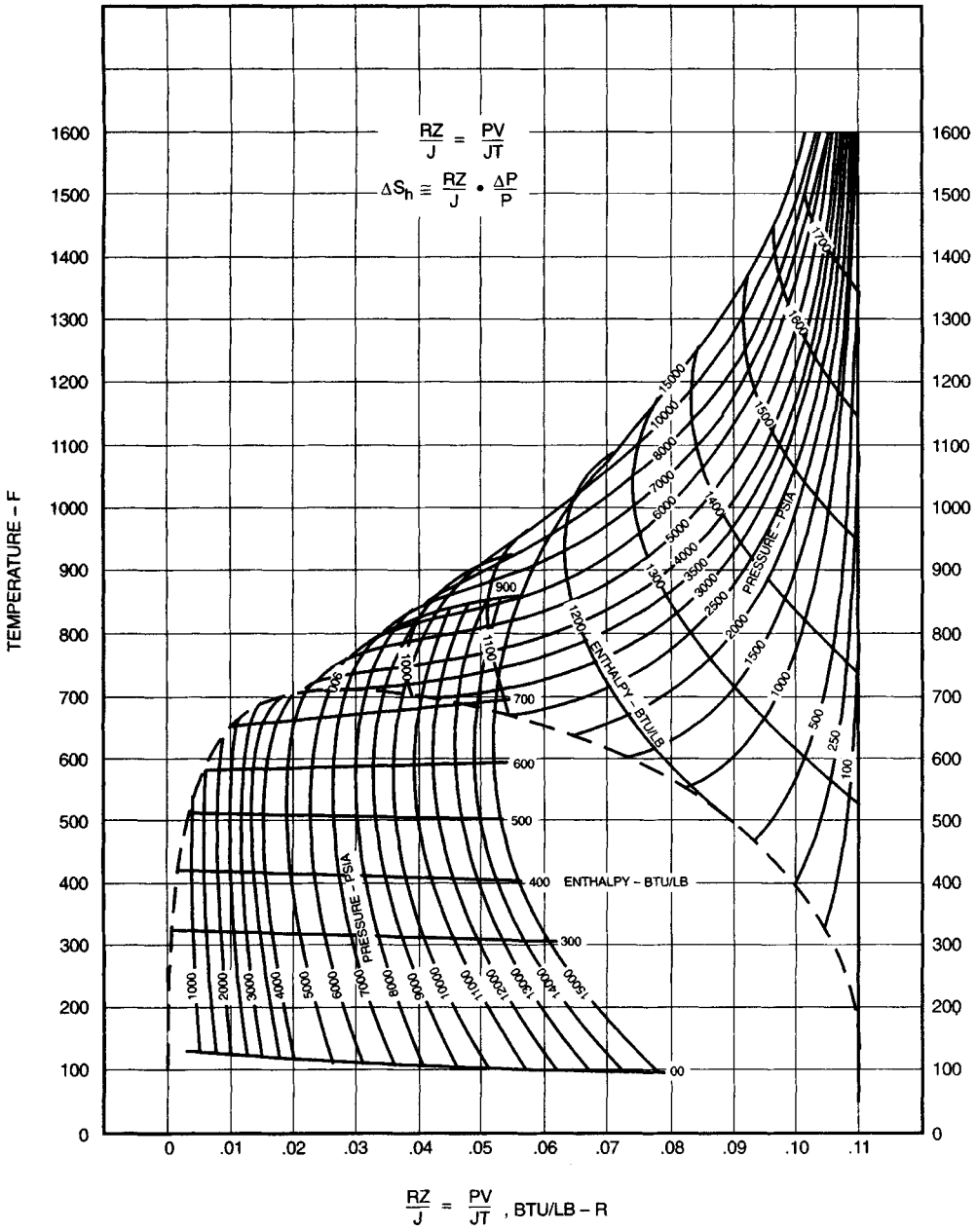

Fig. 58.13 (RZ/J) for steam and water. (From Ref. 5.)

respectively. If the fluid were a perfect gas, this plot would be a straight line. In reality, it is a series of nearly straight lines, with pressure as a parameter. A significant change occurs in the wet steam region, where the pressure parameters spread out at a slope different from that of the superheated region. These plots are quite accurate for determining specific volume and for computing the often used *flow number*

$$\frac{\dot{M}\sqrt{pv}}{p} \tag{58.5}$$

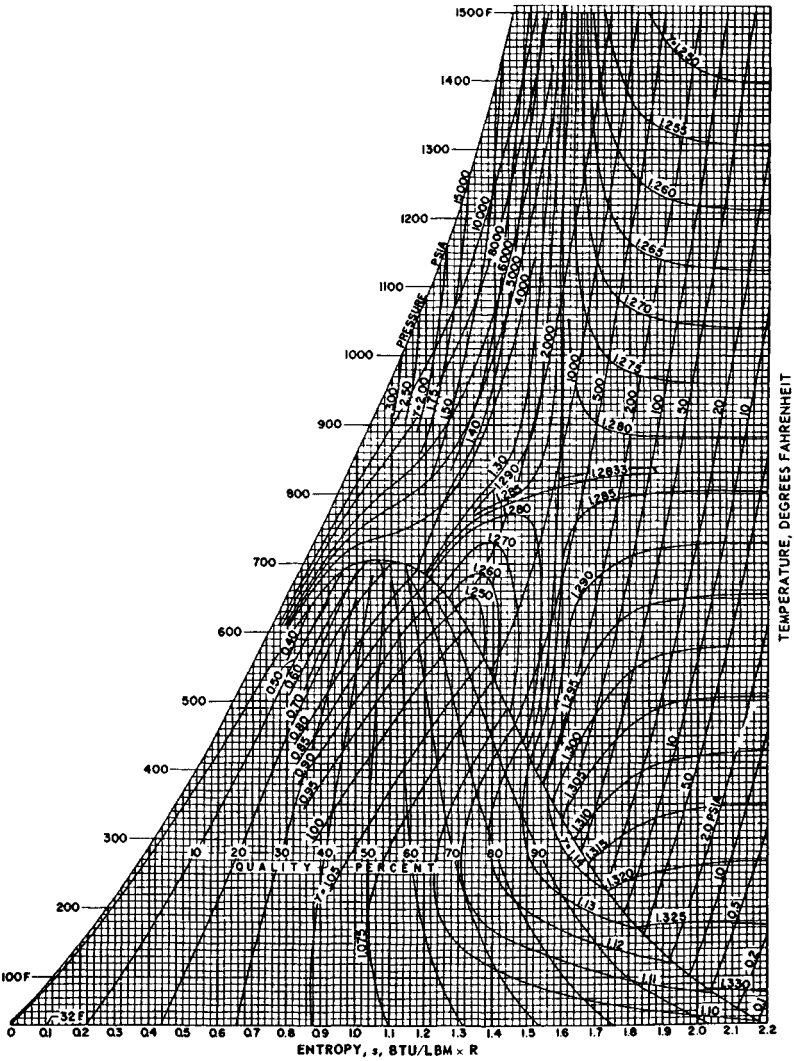

Fig. 58.14 Isentropic exponent, $\gamma = -\frac{v}{p}\left(\frac{\partial p}{\partial v}\right)_s$, pv^γ = constant for a short expansion. (From Ref. 2.)

A direct application of the above-mentioned approximations is the treatment by perfect gas analysis techniques of applications where the working fluid is a mixture of air and a significant amount of steam (*significant* implies greater than 2–4%). Not to limit the application to air and steam, the working fluid could be the products of combustion and steam, or other arbitrary gases and steam.

58.4 BLADE PATH DESIGN

The accomplishment of the thermal to mechanical energy-conversion process in a steam turbine is, in general, achieved by successive expansion processes in alternate stationary and rotating blade rows. The turbine is a heat engine, working between the thermodynamic boundaries of maximum and minimum temperature levels, and as such is subject to the laws of thermodynamics prohibiting the achievement of engine efficiencies greater than that of a Carnot cycle. The turbine is also a dynamic machine in that the thermal to mechanical energy-conversion process depends on blading forces, traveling at rotor velocities, developed by the change of momentum of the fluid passing

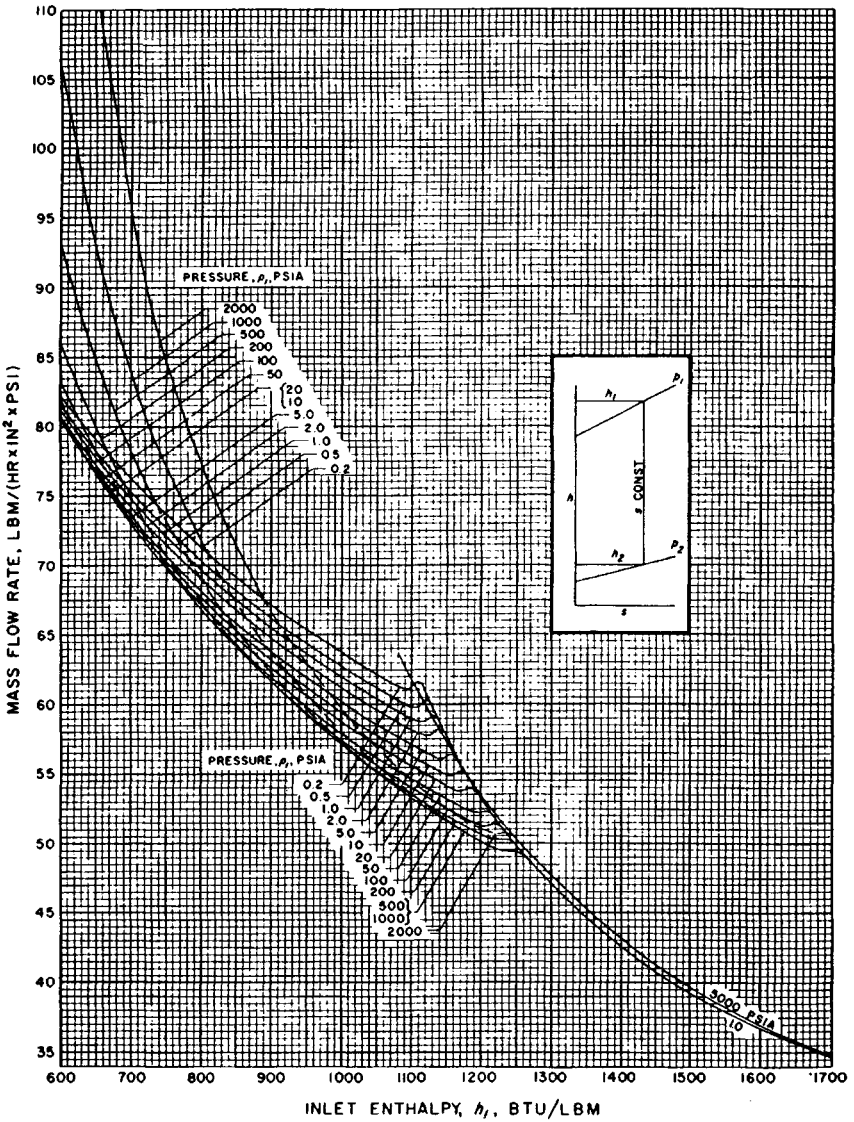

Fig. 58.15 Critical (choking) mass flow rate for isentropic process and equilibrium conditions. (From Ref. 2.)

through a blade passage. The laws of nature as expressed by Carnot and Newton govern the turbine designer's efforts and provide common boundaries for his achievements.

The purpose of this section is to present the considerations involved in the design of steam turbine blade paths and to indicate means by which these concerns have been resolved. The means of design resolution are not unique. An infinite number of possibilities exist to achieve the specific goals, such as efficiency, reliability, cost, and time. The real problem is the achievement of all these goals simultaneously in an optimum manner, and even then, there are many approaches and many very similar solutions.

58.4.1 Thermal to Mechanical Energy Conversion

The purpose of turbomachinery blading is the implementation of the conversion of thermal energy to mechanical energy. The process of conversion is by means of curved airfoil sections that accept

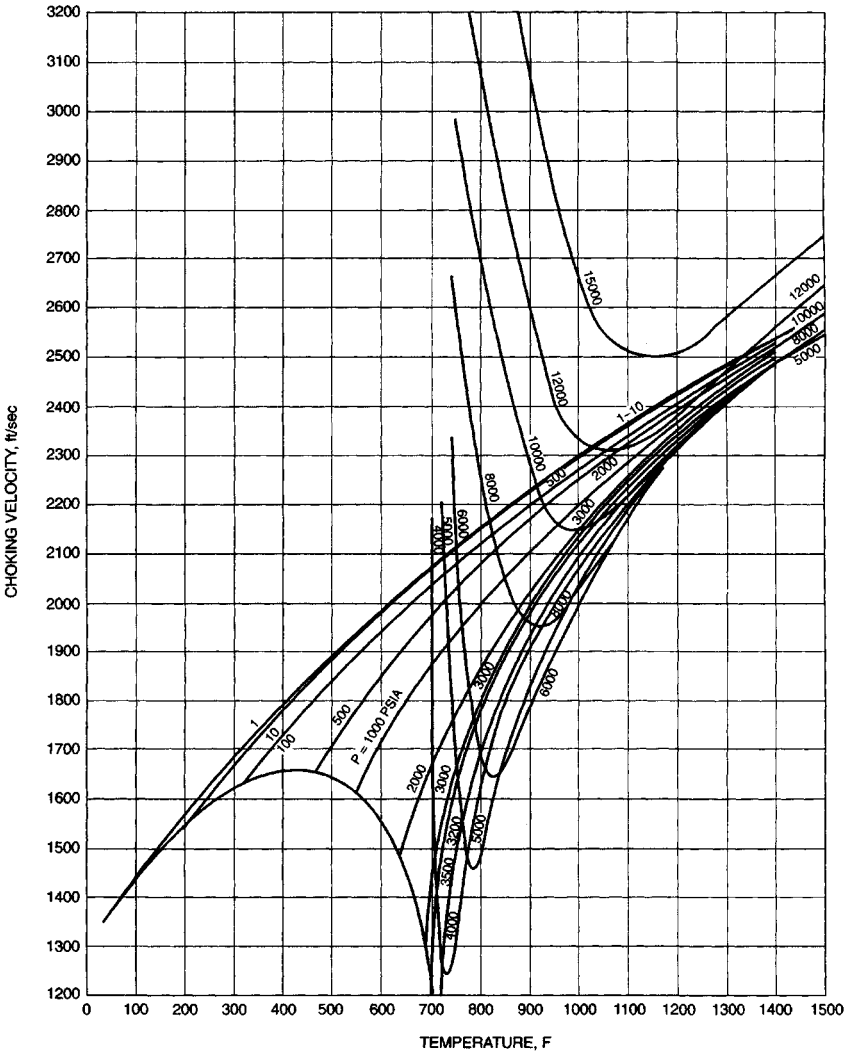

Fig. 58.16 Choking (sonic) velocity as a function of temperature and pressure.

incoming steam flow and redirect it in order to develop blading forces and resultant mechanical work. The force developed on the blading is equal and opposite to the force imposed on the steam flow, that is, the force is proportional to the change of fluid momentum passing through the turbine blade row. The magnitude of the force developed is determined by application of Newton's laws to the quantity of fluid occupying the flow passage between adjacent blades, a space that is in effect, a *streamtube.* The assumptions are made that the flow process is steady and that flow conditions are uniform upstream and downstream of the flow passage.

Figure 58.20 presents an isometric view of a turbine blade row defining the components of steam velocity at the inlet and exit of the blade passage streamtube. The tangential force impressed on the fluid is equal to the change of fluid momentum in the tangential direction by direct application of Newton's laws.

$$F_{\theta \text{on fluid}} = \int_{A_2} V_\theta d\dot{M} - \int_{A_1} V_\theta \, d\dot{M} \tag{58.6}$$

$$F_{\theta \text{on fluid}} = \int_{A_2} \rho_2 V_{Z2} V_{\theta_2} \, dA - \int_{A_1} \rho_1 V_{Z1} V_{\theta_1} \, dA \tag{58.6a}$$

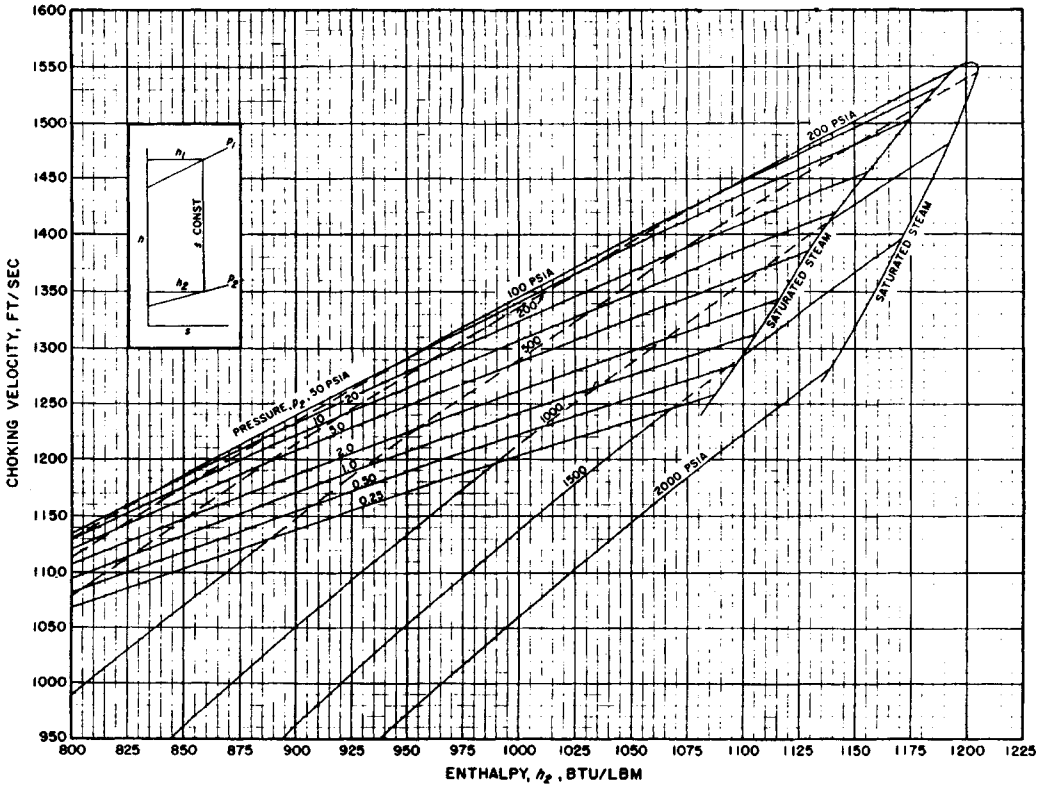

Fig. 58.17 Choking velocity for water–steam mixture for isentropic process and equilibrium conditions. (From Ref. 2.)

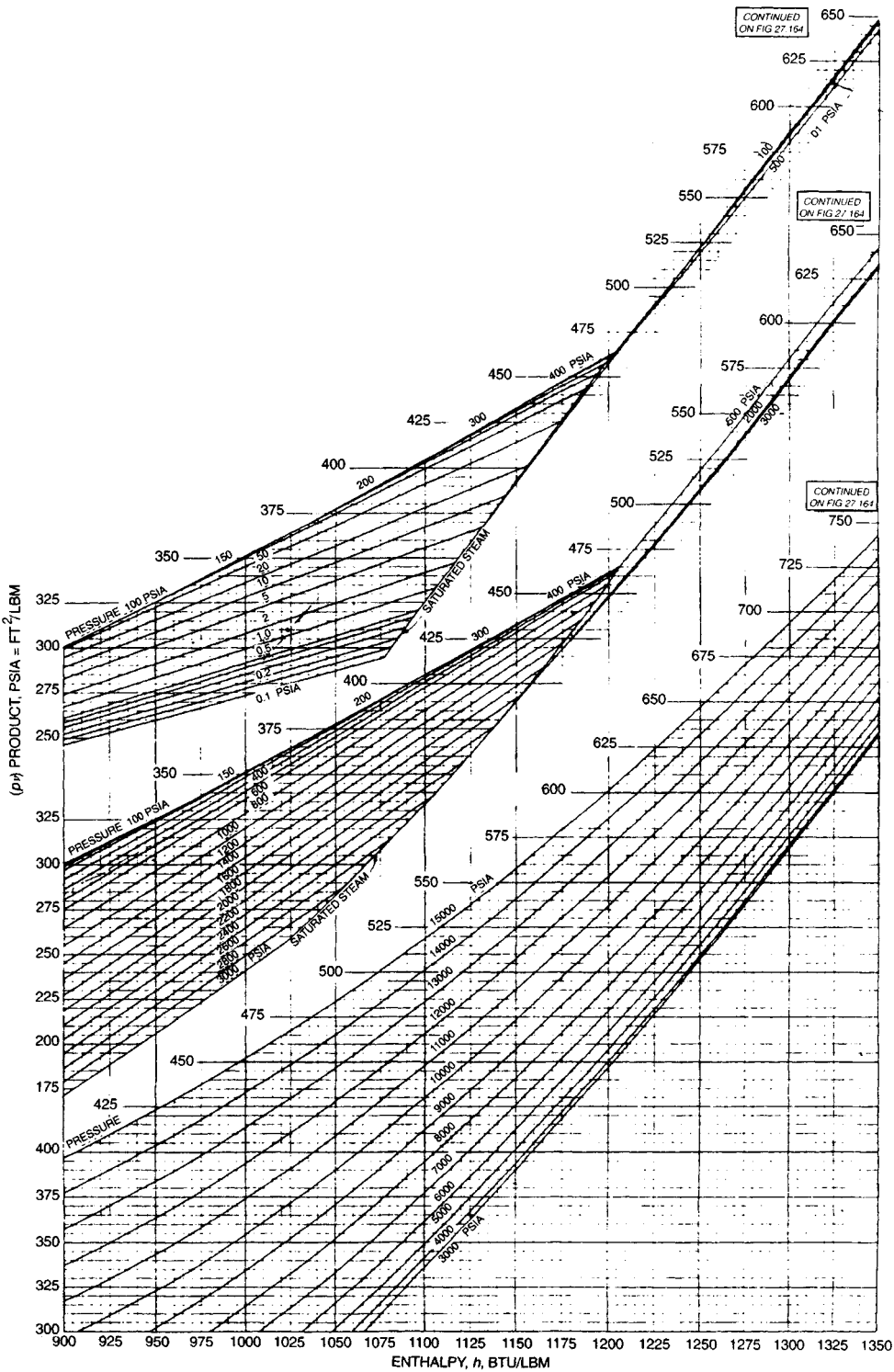

Fig. 58.18 (ρv) product for low-temperature steam. (From Ref. 2.)

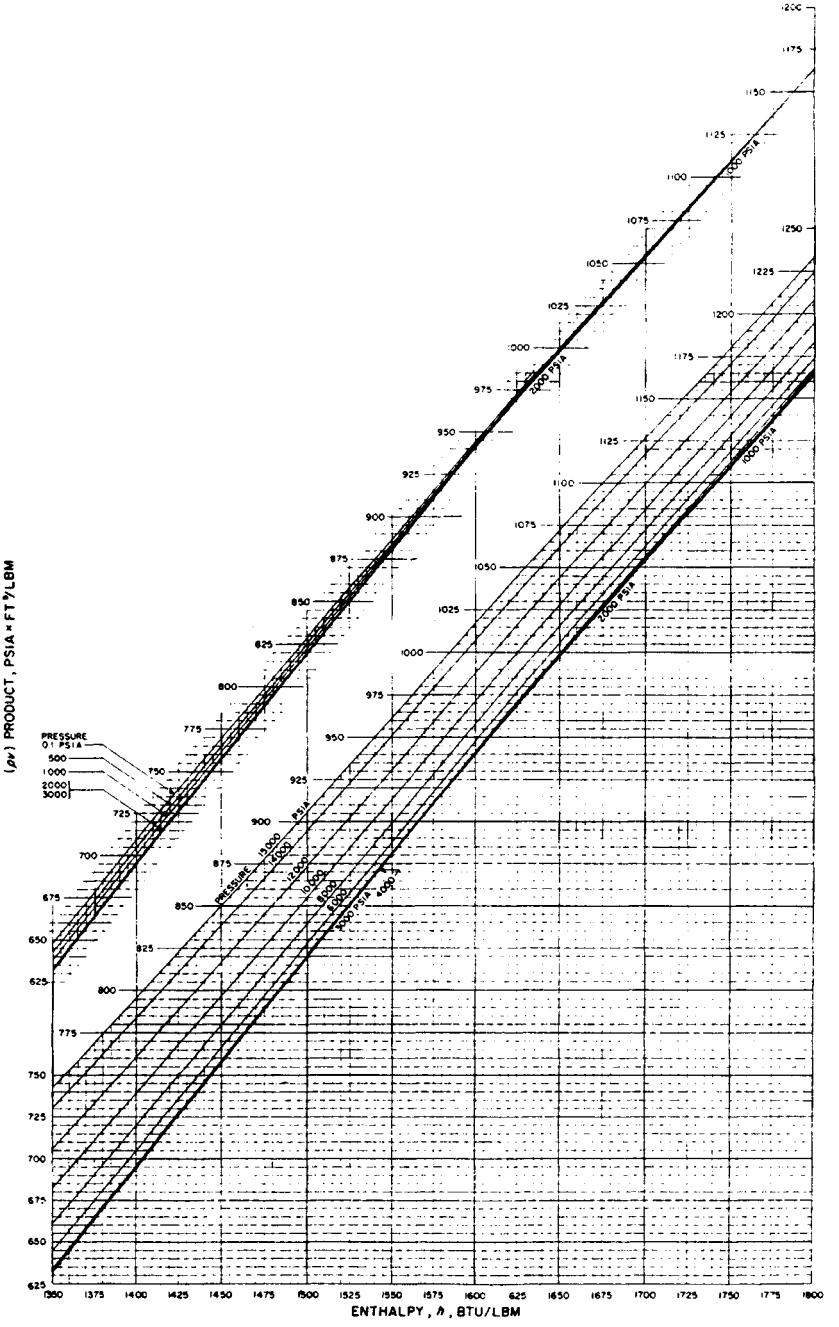

Fig. 58.19 (ρv) product for high-temperature steam. (From Ref. 2.)

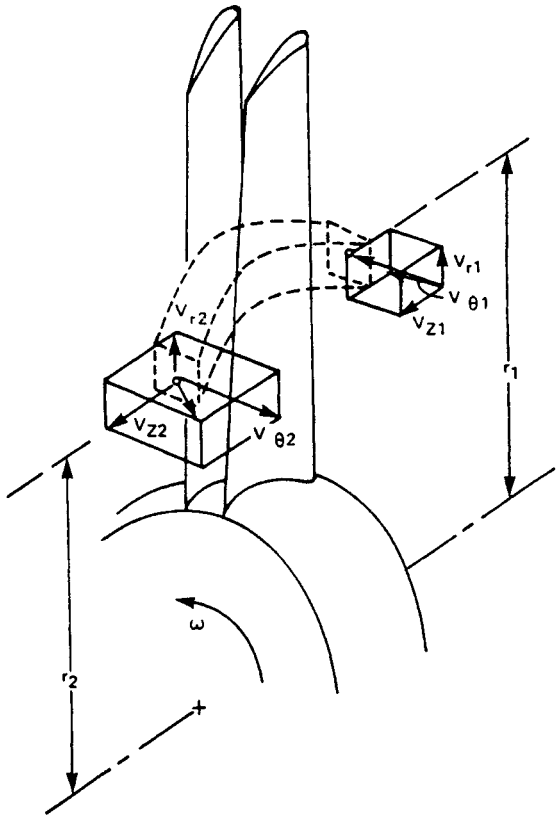

Fig. 58.20 Turbine blade row streamtube.

Since the flow is assumed steady and the velocity components are assumed constant within the streamtube upstream and downstream of the blade row, the force on the fluid is

$$F_{\theta \text{on fluid}} = \frac{\dot{M}}{g}(V_{\theta_2} - V_{\theta_1}) \tag{58.6b}$$

If the entering and leaving streamtube radii are identical, the power P developed by the moving blade row is

$$P = \frac{\dot{M}}{g} r\omega(V_{\theta 1} - V_{\theta 2}) \tag{58.7}$$

where the algebraic sign is changed to determine the fluid force on the blade. With unequal radii, implying unequal tangential blade velocities, the change in angular fluid momentum requires the power relation to be

$$P = \frac{\dot{M}}{g} \omega(r_1 V_{\theta 1} - r_2 V_{\theta 2}) \tag{58.7a}$$

Consideration of the general energy relationship (the First Law) expressed as

$$\delta Q - \delta W = du + d(pv) + \frac{VdV}{g} + dz \tag{58.8}$$

(Q is heat, W is work, and u is internal energy) and applied to the inlet and exit of the streamtube yields

$$\delta W = dh + \frac{VdV}{g} = dh_0 \tag{58.9}$$

where h is static enthalpy and h_0 is stagnation enthalpy. The change in total energy content of the fluid must equal that amount absorbed by the moving rotor blade in the form of mechanical energy

$$h_{01} - h_{02} = \frac{\omega}{g}(r_1 V_{\theta 1} - r_2 V_{\theta 2}) \tag{58.10}$$

or

$$h_1 + \frac{V_1^2}{2g} - h_2 - \frac{V_2^2}{2g} = \frac{\omega}{g}(r_1 V_{\theta 1} - r_2 V_{\theta 2}) \tag{58.10a}$$

Both of these may be recognized as alternate forms of *Euler's turbine equation.*

In the event the radii r_1 and r_2 are the same, Euler's equation may be expressed in terms of the velocity components relative to the rotor blade as

$$h_{01} - h_{02} = \frac{U}{g}(W_{\theta 1} - W_{\theta 2}) \tag{58.10b}$$

or

$$h_1 + \frac{V_1^2}{2g} - h_2 - \frac{V_2^2}{2g} = \frac{U}{g}(W_{\theta 1} - W_{\theta 2}) \tag{58.10c}$$

58.4.2 Turbine Stage Designs

The means of achieving the change in tangential momentum, and hence blade force and work, are many and result in varying turbine stage designs. Stage design and construction falls generally into two broad categories, *impulse* and *reaction.* The former implies that the stage pressure drop is taken entirely in the stationary blade passage, and that the relative entering and leaving rotor blade steam velocities are equal in magnitude. Work is achieved by the redirection of flow through the blade without incurring additional pressure decrease. At the other end of the scale, one could infer that for the reaction concept, all the stage pressure drop is taken across the rotor blade, while the stator blade merely redefines steam direction. The modern connotation of reaction is that of 50% *reaction,* wherein half the pressure drop is accommodated in both stator and rotor. Reaction can be defined in two ways, on an enthalpy-drop or a pressure-drop basis. Both definitions ratio the change occurring in the rotor blade to the stage change. The pressure definition is more commonly encountered in practice.

Figure 58.21 presents a schematic representation of impulse and reaction stage designs. The impulse design requires substantial stationary diaphragms to withstand the stage pressure drop and tight sealing at the inner diameter to minimize leakage. The reaction design (50%) can accept somewhat greater seal clearances under the stator and over the rotor blade and still achieve the same stage efficiency.

The work per stage potential of the impulse design is substantially greater than that of the reaction design. A comparison is presented in Fig. 58.22 of various types of impulse designs with the basic 50% reaction design. A typical impulse stage (*Rateau stage*) can develop 1.67 times the work output of the reaction stage; for a given energy availability, this results in 40% fewer stages.

Performance characteristics of these designs are fundamentally described by the variation of stage aerodynamic efficiency as a function of velocity ratio. The *velocity ratio* can be defined many ways dependent on the reference used to define the steam speed V. The velocity ratio in general is

$$\nu = \frac{U}{V} \tag{58.11}$$

where U is the blade tangential velocity.

The relative level of stage aerodynamic efficiency is indicated in Fig. 58.22 for these various geometries ranging from the symmetrical reaction design (50% reaction) to a three-rotating-row impulse design. As the work level per design increases, the aerodynamic efficiency decreases. Some qualifying practicalities prevent this from occurring precisely this way in practice. That is, the impulse concept can be utilized in the high-pressure region of the turbine, where densities are high and blade heights are short. When blade heights necessarily increase in order to pass the required mass flow, significant radial changes occur in the flow conditions, resulting in radial variations in pressure and, hence, reaction. All impulse designs have some amount of reaction dependent on the ratio of blade

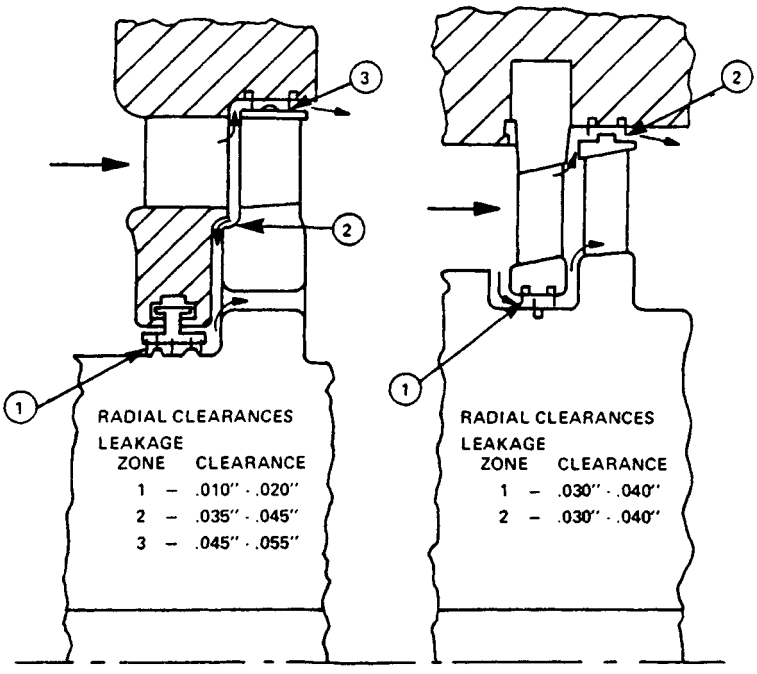

Fig. 58.21 Comparison of impulse and reaction stage geometries: (*a*) impulse construction; (*b*) reaction construction.

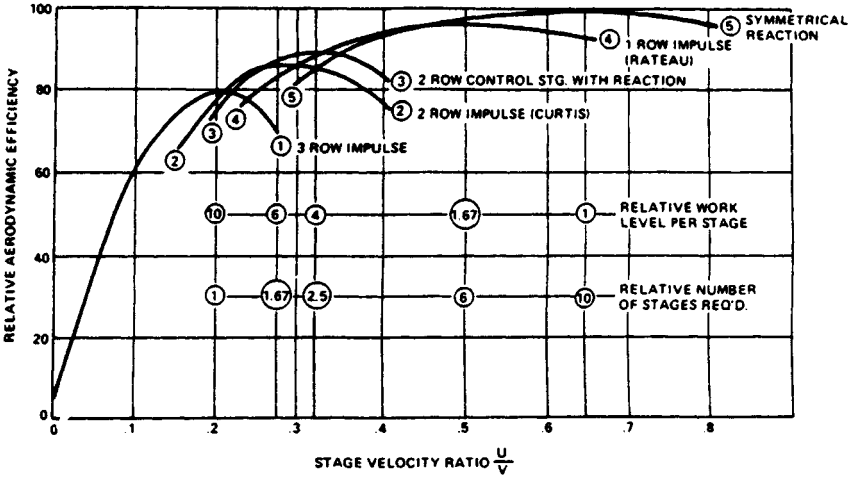

Fig. 58.22 The effect of stage design on aerodynamic efficiency.

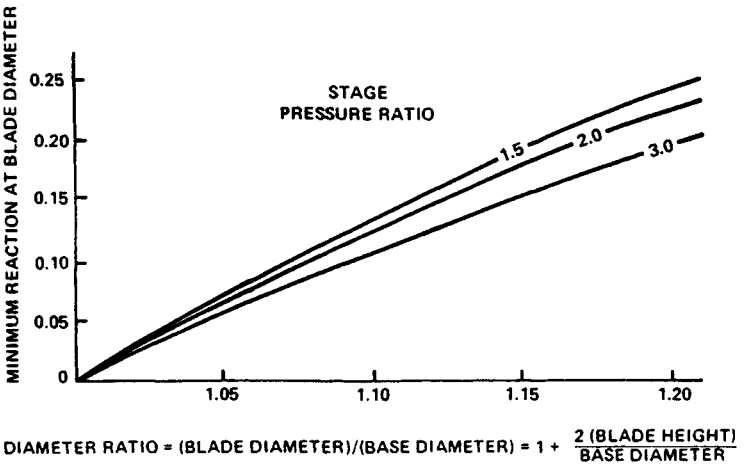

Fig. 58.23 Blade reaction required to prevent negative base reaction.

hub to tip diameters. Figure 58.23 presents the variation of reaction in a typical impulse stage as a function of the blade diameter/base diameter ratio.

Further complications arise when comparing the impulse to the reaction stage design. The rotor blade turning is necessarily much greater in the impulse design, the work done can be some 67% greater, and the attendant blade section aerodynamic losses tend to be greater. As an extreme case, Fig. 58.24 presents blade losses as a function of turning angle, indicating much greater losses incurred by the impulse rotor blade design.

Test data is, of course, the best source of information defining these performance relationships. Overall turbine test data provide the stage characteristic, which includes all losses incurred. The fundamental blade section losses are compounded by leakages around blade ends, three-dimensional losses due to finite length blades and their end walls, moisture losses if applicable, disk and shroud friction, and blading incidence losses induced by the variation in the velocity ratio itself. A detailed description of losses has been presented by Craig and Cox[6] and more recently by others including Kacker and Okapuu.[7]

58.4.3 Stage Performance Characteristics

Referring again to Fig. 58.20, the velocities relative to the rotor blade are related to the stator velocities and to the wheel speed by means of the appropriate velocity triangles, as in Fig. 58.25.

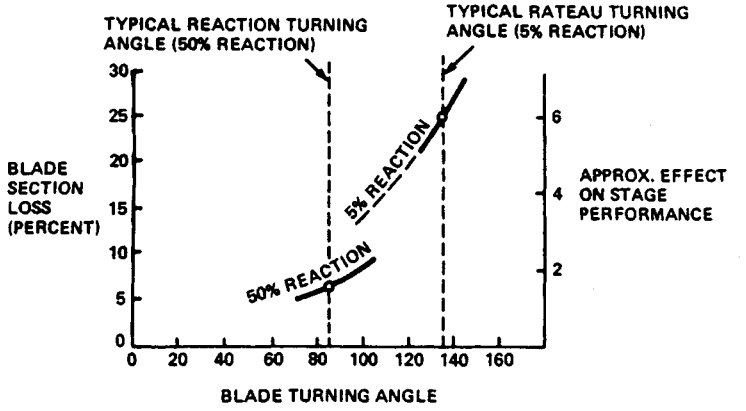

Fig. 58.24 Blade section losses as a function of turning and reaction.

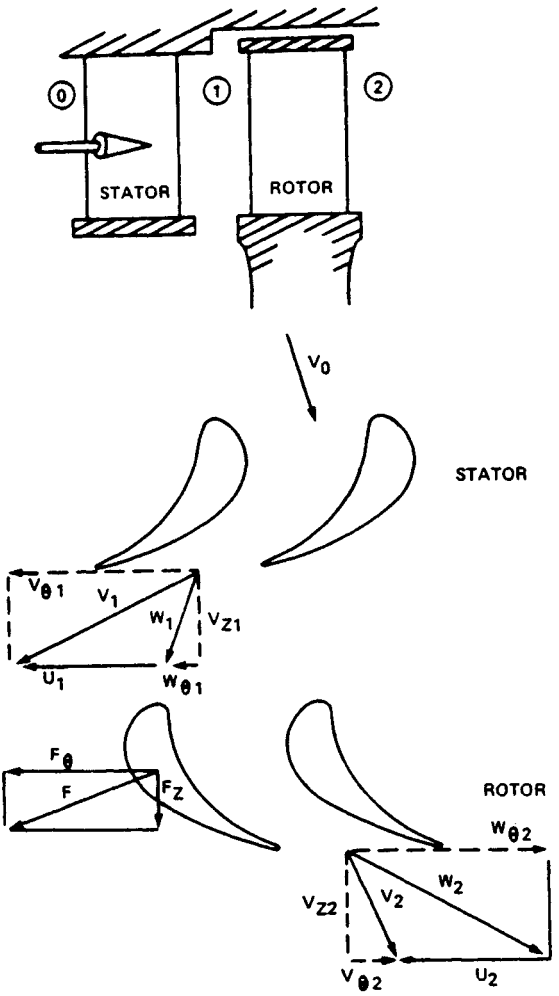

Fig. 58.25 Stage velocity triangles.

Absolute velocities are denoted by V and relative velocities by W. The blade sections schematically shown in this figure are representative of reaction blading. The concepts and relationships are representative of all blading.

The transposition of these velocities and accompanying steam conditions are presented on a Mollier diagram for superheated steam in Fig. 58.26. The stage work will be compatible with Euler's turbine equation shown in Eqs. (58.10). The *stage work* is the change in total enthalpy ($\Delta h_w = h_{00} - h_{02}$) of the fluid passing through the stage. The total pressures and temperatures before and after the stage, the local thermodynamic conditions, and total pressure and total temperature relative to the rotor blade (p_{0_r} and T_{0_r}) are all indicated in Fig. 58.26.

This ideal description of the steam expansion process defines the local conditions of a particular streamtube located at a certain blade height. For analysis calculations and the prediction of turbine performance, the mean diameter is usually chosen as representative of the stage performance. This procedure is, in effect, a one-dimensional analysis, and it represents the turbine performance well if appropriate corrections are made for three-dimensional effects, leakage, and moisture. In other words, the blade row, or stage efficiency, must be known or characterized as a function of operating parameters. The velocity ratio, for example, is one parameter of great significance. Dimensional analysis of the individual variables bearing on turbomachinery performance has resulted in several commonly used dimensionless quantities:

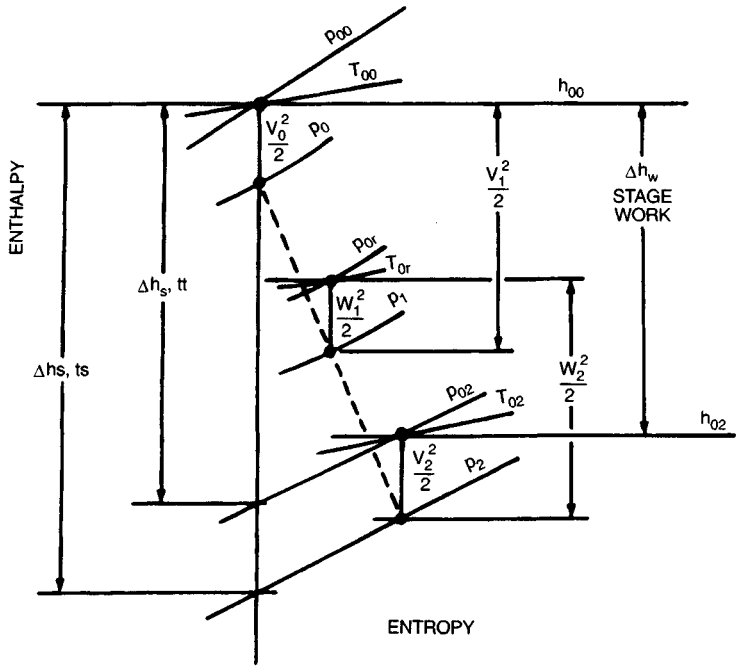

Fig. 58.26 Stage thermodynamic conditions on a Mollier diagram.

$$\nu = \text{velocity ratio } (U/V) \tag{58.12}$$

$$\rho = \text{pressure ratio } (p_0/p) \tag{58.13}$$

$$\frac{\dot{M}\sqrt{\theta}}{\delta} = \text{referred flow rate} \tag{58.14}$$

$$\frac{N}{\sqrt{\theta}} = \text{referred speed} \tag{58.15}$$

$$\eta = \text{efficiency} \tag{58.16}$$

where $\theta = T_0/T_{\text{ref}}$ and $\delta = p_0/p_{\text{ref}}$.

The *referred flow rate* is a function of pressure ratio. In gas dynamics, the referred flow rate through a converging nozzle is primarily a function of the pressure ratio across the nozzle (Fig. 58.27). When the pressure ratio p_0/p is approximately 2 (depending on the ratio of specific heats), the referred mass flow maximizes, that is,

$$\frac{\dot{M}\sqrt{T_0}}{p_0} = \text{constant} \tag{58.17}$$

This referred flow rate is also termed a *flow number* and takes the following form, which is more appropriate for steam turbine usage.

$$\frac{\dot{M}\sqrt{p_0 v_0}}{p_0} = \text{flow number} \tag{58.18}$$

The turbine behaves in a manner similar to a nozzle, but it is also influenced by the wheel-speed Mach number, which is represented by $N/\sqrt{T_0}$. In effect, a similar flow rate–pressure ratio relationship is experienced, as shown schematically in Fig. 58.28.

A combined plot describing turbine performance as a function of all these dimensionless quantities is shown schematically in Fig. 58.29. Power-producing steam turbines, however, run at constant speed and at essentially constant flow number, pressure ratio, and velocity ratio, and in effect operate at

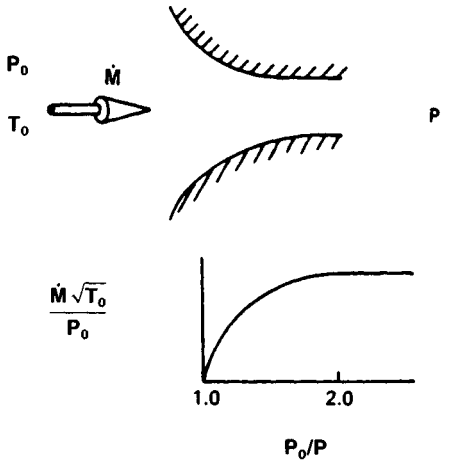

Fig. 58.27 Gas dynamic flow relationships.

nearly a fixed point on this performance map. Exceptions to this are the control stage, if the unit has one, and the last few stages of the machine. The control stage normally experiences a wide range of pressure ratios in the situation where throttle pressure is maintained at a constant value and a series of governing valves admits steam to the control stage blading through succeeding active nozzle arcs.

The last stage of the low pressure end exhausts to an essentially constant pressure zone maintained by the condenser. Some variation occurs as the condenser heat load changes with unit flow rate and load. At a point several stages upstream where the pressure ratio to the condenser is sufficiently high, the flow number is maintained at a constant value. As unit load reduces, the pressure level and mass flow rate decrease simultaneously and the pressure ratio across the last few stages reduces in value. This change in pressure ratio changes the stage velocity ratio, and the performance level of these last few stages change. Figure 58.30 indicates the trend of operation of these stages as a function of load change superimposed on the dimensionless turbine performance map. It is these last few stages, say two or three, that confront the steam turbine designer with the greatest challenge.

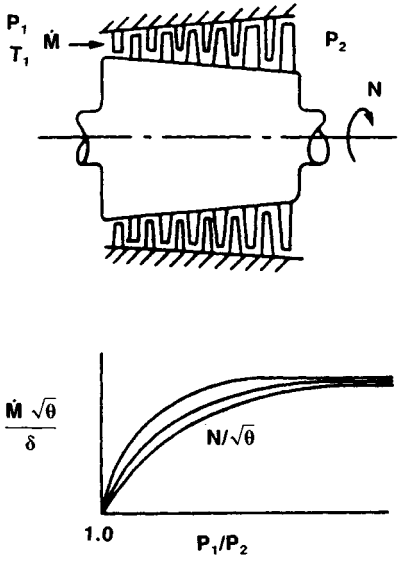

Fig. 58.28 Turbine flow relationships.

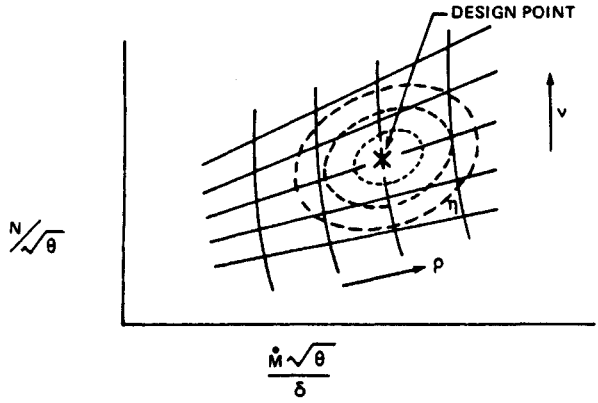

Fig. 58.29 Turbine performance map.

58.4.4 Low-Pressure Turbine Design

The low-pressure element of the steam turbine is normally a self-contained design, in the sense that it comprises a rotor carrying several stages, a cylinder with piping connections, and bearings supporting the rotor. Complete power-generating units may use from one to three low-pressure elements in combination with high-pressure and intermediate-pressure elements depending on the particular application.

Symmetric double-flow designs utilize from 5 to 10 stages on each end of the low-pressure element. The initial stage accepts flow from a centrally located plenum fed by large-diameter, low-pressure steam piping. In general, the upstream stages feature constant cross-section blading, while the latter stages require blades of varying cross section. Varying design requirements and criteria result in these latter twisted and tapered low pressure blades comprising from 40 to 60% of the stages in the elements.

The particular design criterion used significantly affects the end product. For example, the low-pressure end (one-half of the element) of a nuclear unit might contain 10 stages and rotate at 1800 rpm and generate 100 mW, while the fossil machine would spin at 3600 rpm, carry five or six stages, and develop 50 mW. The physical size could double and the weight increase by a factor of 8.

Further differences in design are immediately implied by the steam conditions to be accepted by the element. The nuclear unit inlet temperature would be approximately 550°F (288°C), as compared to the fossil condition of 750°F (399°C). The nuclear unit must also be designed to effectively remove blade path moisture in order to achieve high thermal performance levels (heat rate). Moisture-removal devices in both the high-pressure and low-pressure elements are normally incorporated for this purpose. Blading physical erosion is also an important consideration. Material removal by the high speed

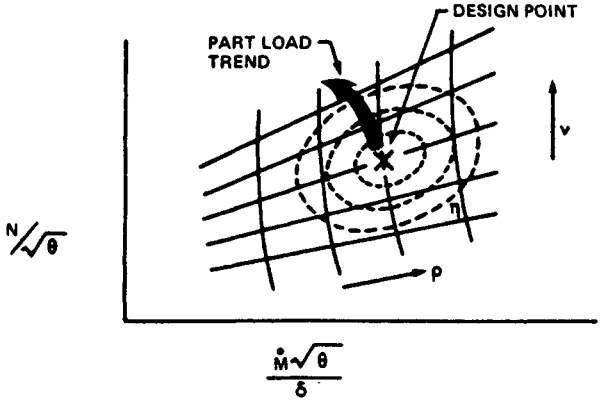

Fig. 58.30 Turbine performance map with part load trend.

impingement of water droplets can be minimized by proper design. Moore and Sieverding[8] describe the phenomena controlling wet steam flow in turbines.

Flow Field Considerations

Substantial advances have been achieved in the aerothermodynamic processes of low-pressure turbines. A significant factor is the availability of high-speed digital computers in the solution of the system of turbomachinery aerothermodynamic equations. The coupling of the solution of this complex equation system with the necessary verification as derived from experimental testing programs is the subject of this section.

The development of the system of aerothermodynamic equations is traced from basic considerations of the several conservation equations to working equations, which are then generally solved by numerical techniques. Pioneering work in the development of this type of equation systems was performed by Wu.[9] Subsequent refinement and adaptation of his fundamental approach has been made by several workers in recent years.

The general three-dimensional representation of the conservation equations of mass, momentum, and energy can be written for this adiabatic system

$$\frac{\partial \rho}{\partial t} + \nabla \cdot \rho \overline{\mathrm{V}} = 0 \tag{58.19}$$

$$\frac{\partial \overline{\mathrm{V}}}{\partial t} + \overline{\mathrm{V}} \cdot \nabla \overline{\mathrm{V}} = -\frac{1}{\rho} \nabla p \tag{58.20}$$

$$\nabla h = T \nabla s + \frac{1}{\rho} \nabla p \tag{58.21}$$

Assuming the flow to be steady and axisymmetric, the conservation equations can be expanded in cylindrical coordinates as

$$\frac{\partial}{\partial r} (\rho r b V_r) + \frac{\partial}{\partial z} (\rho r b V_z) = 0 \tag{58.22}$$

$$V_r \frac{\partial}{\partial r} (r V_\theta) + V_z \frac{\partial}{\partial z} (r V_\theta) = 0 \tag{58.23}$$

$$V_r \frac{\partial V_z}{\partial r} + V_z \frac{\partial V_z}{\partial z} = -\frac{1}{\rho} \frac{\partial p}{\partial z} \tag{58.24}$$

$$V_r \frac{\partial V_r}{\partial r} + V_z \frac{\partial V_r}{\partial z} - \frac{V_\theta^2}{r} = -\frac{1}{\rho} \frac{\partial p}{\partial r} \tag{58.25}$$

$$\frac{1}{\rho} dp = dh_0 - Tds - \frac{1}{2} d(V_\theta^2 + V_z^2 + V_r^2) \tag{58.26}$$

where

$$h_0 = h + \tfrac{1}{2}(V_\theta^2 + V_z^2 + V_r^2) \tag{58.27}$$

and b has been introduced to account for *blade blockage.* The properties of steam may be described by equations of state, such that $p = p\ (p, T)$ and $h = h\ (p, T)$. These functions are available in the form of the steam tables.[2]

As the increase in system entropy is a function of the several internal loss mechanisms inherent in the turbomachine, it is necessary that definitive known (or assumed) relationships be employed for its evaluation. In the design process, this need can usually be met, while the performance analysis of a given geometry usually introduces loss considerations more difficult to evaluate completely. The matter of loss relationship has been discussed with regard to stage design and will be further reviewed in a later section. In general, however, the entropy increase can be determined as a function of aerodynamic design parameters, that is,

$$\Delta s = f(V_i, W_i, \text{Mach number}) \tag{58.28}$$

Equations (58.22) through (58.25) form a system of nine equations in nine unknowns, V_r, V_θ, V_z, ρ, p, T, h, h_0, and s, the solution of which defines the low pressure turbine flow field.

The *meridional plane*, defined as that plane passing through the turbomachine axis and containing the radial and axial coordinates, can be used to describe an additional representation of the flow process. The velocity V_m (see Fig. 58.31) represents the streamtube meridional plane velocity with direction proportional to the velocity components V_r and V_z. If the changes in entropy and total enthalpy along the streamlines are known, or specified, it can be shown that Eqs. (58.24) and (58.25) are equivalent and that Eq. (58.23) is also satisfied. Application of Eq. (58.22) to the rotating blade in effect described Euler's turbine equation when equated to the blade force producing useful work. In this situation, it is most convenient to choose Eq. (58.25), the commonly known *radial equilibrium equation,* as the relationship for continued evaluation.

58.4.5 Flow Field Solution Techniques

Two commonly encountered techniques have been employed to solve this set of fundamental differential equations and relationships. They are usually referred to as the *streamline curvature* and *matrix solution* techniques. The streamline curvature technique is structured to evaluate meridional velocities and to trace streamlines in the flow field, allowing the calculation of the streamline curvature itself. The streamline curvature technique has been developed to a high degree of sophistication and has been applied to axial flow compressor design as well as to axial flow turbine problems.

The matrix approach utilizes a stream function satisfying the equation of continuity. The calculation procedure then determines the stream function throughout the flow field. This technique has also been developed satisfactorily with particular application to low-pressure steam turbines. The matrix approach asserts the existence of a stream function that is defined such that

$$V_r = -\frac{1}{\rho r b}\frac{\partial \psi}{\partial z} \tag{58.29}$$

and

$$V_z = \frac{1}{\rho r b}\frac{\partial \psi}{\partial r} \tag{58.30}$$

With this definition, ψ, V_r, and V_z identically satisfy Eq. (58.19). The combination of the equations of momentum, energy, and continuity, Eqs. (58.25), (58.26), (58.29), (58.30), and the definition of total enthalpy, Eq. (58.27), results in

$$\frac{\partial}{\partial r}\left(\frac{1}{\rho r b}\frac{\partial \psi}{\partial r}\right) + \frac{\partial}{\partial z}\left(\frac{1}{\rho r b}\frac{\partial \psi}{\partial z}\right) = \frac{1}{V_z}\left[\frac{\partial h_o}{\partial r} - \frac{V_\theta}{r}\frac{\partial (r V_\theta)}{\partial r} - T\frac{\partial s}{\partial r}\right] \tag{58.31}$$

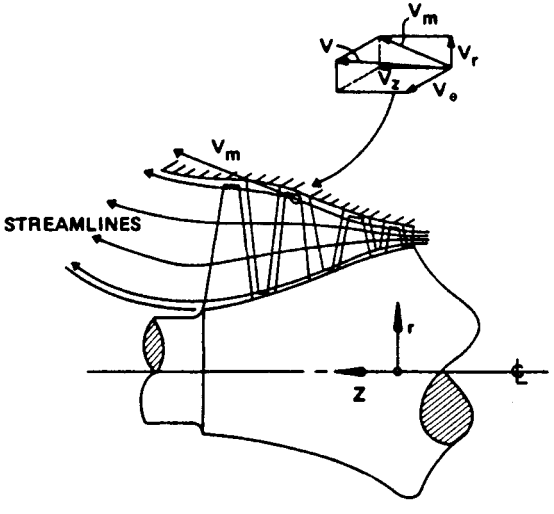

Fig. 58.31 Turbine blade path flow field.

This is the basic flow field equation, which can then be solved by numerical techniques. This equation is an elliptic differential equation, provided the meridional Mach number is less than unity. This is probably the case in all large steam turbines. The absolute Mach number can of course exceed unity and usually does in the last few blade rows of the low-pressure turbine.

The streamline curvature approach satisfies the same governing equations but solves for the meridional velocity V_m rather than the stream function ψ, as in the matrix approach. Equations (58.25) and (58.26) can be combined and expressed in terms of directions along the blade row leading or trailing edges. An equation used to describe the variation of meridional velocity is

$$\frac{dV_m^2}{dl} + A(l)V_m^2 = B(l) \tag{58.32}$$

where l is the coordinate along the blade edge and the coefficients A and B depend primarily on the slopes of the streamlines in the meridional plane. An iterative process is then employed to satisfy the governing equations.

58.4.6 Field Test Verification of Flow Field Design

The most conclusive verification of a design concept is the in-service evaluation of the product with respect to its design parameters. Application of a matrix-type flow field design program has been made to the design of the last three stages of a 3600-rpm low-pressure end. Figure 58.32 is indicative of the general layout of this high-speed fossil turbine.

The aerodynamic design process is to a great degree an iterative process, that is, the specification of the design parameters (for example, work per stage and radial work distribution) are continuously adjusted in order to optimize the flow field design. Just as important, feedback from mechanical analyses must be accommodated in order to achieve reliable long low-pressure blades.

A key design criterion is the requirement that low-pressure blades must be vibrationally tuned in that the lowest several natural modes of vibration must be sufficiently removed from harmonics of running speed during operation. This tuning process is best represented by the *Campbell diagram* of Fig. 58.33. The first four modes of the longest blade are represented as a function of running speed in rpm. At the design speed, the intersection of the mode lines and their band widths indicate nonresonant operation. A comparison is also shown between full-size laboratory test results and shop test data. The laboratory results[10] were obtained by means of strain gage signals transmitted by radio telemetry techniques. In the shop tests, the blades were excited once per revolution by a specially designed steam jet. The strain gage signals were delivered to recording equipment by means of slip rings.

If it turns out that the mode lines intersect a harmonic line at running speed, a resonant condition exists that could lead to a fatigue failure of the blade. The iterative process occurs prior to laboratory

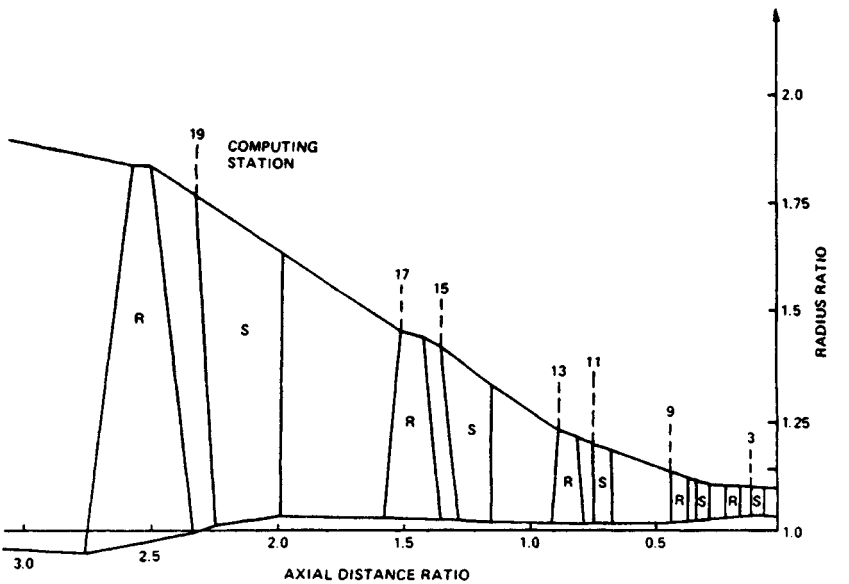

Fig. 58.32 Low-pressure turbine blade path.

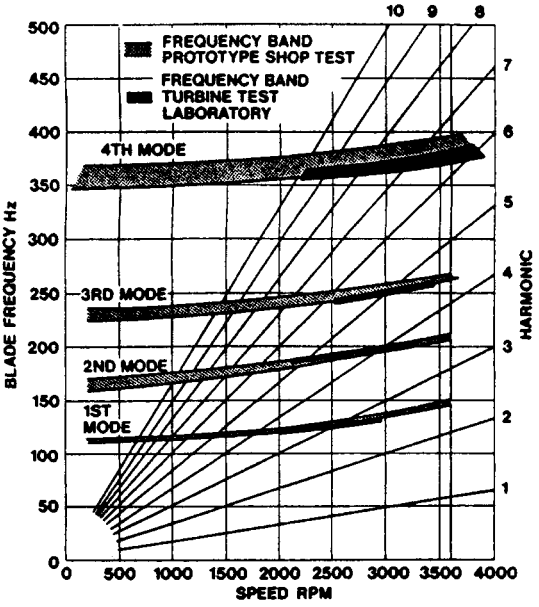

Fig. 58.33 Campbell diagram of low-pressure blade.

and shop verification. Analytic studies and guidance from experience gained from previous blade design programs enable the mechanical designer to determine blade shape changes that will eliminate the resonance problem. This information is then incorporated by the aerodynamicist into the flow field design. As this process continues, manufacturing considerations are incorporated to ensure the design can be produced satisfactorily.

Construction and testing then followed: test data was obtained from several sources, a field test and an in-house test program.[10] Figure 58.34 displays low-pressure turbine efficiency versus exhaust volumetric flow for the advanced design turbine, designed by means of the matrix-type flow field design process, and original design turbine. Although the same range of exhaust volumetric flow was not achievable in both test series, the improvement is apparent and is further indicated by the extended performance line of the original design as determined by predictive techniques.

Field test results were obtained in which the original design and the advanced design were evaluated by procedures defined by the ASME Performance Test Code. Figure 58.35 presents these results in the form of low-pressure turbine efficiency, again as a function of exhaust volumetric flow. The improvement in turbine efficiency is equivalent to 70 Btu/kWh in turbine cycle heat rate (18 kcal/kWh).

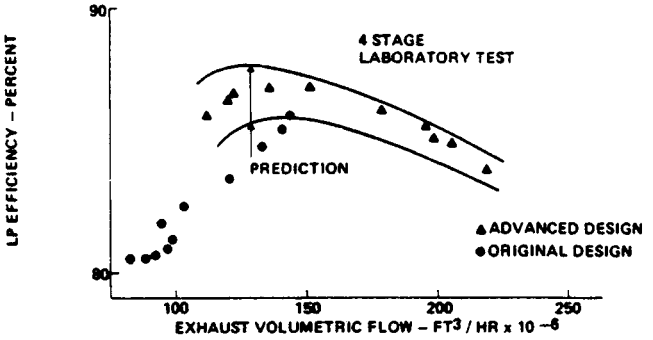

Fig. 58.34 Low-pressure turbine laboratory test results.

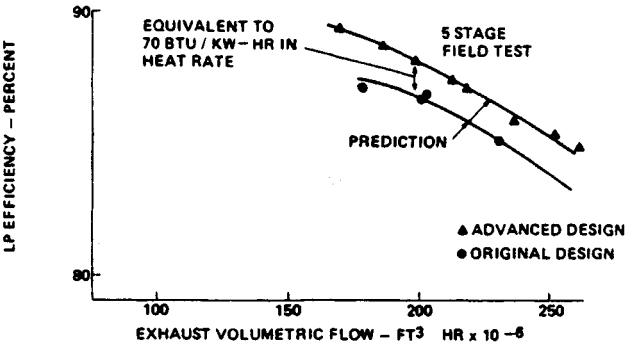

Fig. 58.35 Low-pressure turbine field test results.

Aerodynamic losses in the blade path are an integral part of performance determination, as they directly affect the overall efficiency of the turbine. The losses at part load, or off-design operation, are additive to those existing at the design point and may contribute significantly to a deterioration of performance. Many factors influence these incremental losses, but they are due primarily to blading flow conditions that are different from those at the optimum operating condition. For example, lower (or higher) mass flow rates through the machine have been shown to change the pressure levels, temperatures, velocities, flow angles, moisture content, and so on within the blading. These changes induce flow conditions relative to the blading, which create additional losses. As different radial locations on the same blade are affected to a different degree, the overall effect must be considered as a summation of all individual effects for that blade. In fact, different blade rows, either stationary or rotating, are affected in a like manner, and the complete effect would then be the summation of the individual effects of all the blade rows.

Detailed verification of the design process has been obtained from the analysis and comparison of these internal flow characteristics to expected conditions, as determined by off-design calculations employing the same principles as incorporated in the design procedure. From measurements of total and static pressure and a knowledge of the enthalpy level at the point of interest, it is possible to determine the steam velocity, Mach number, and local mass flow rate. The flow angle is measured simultaneously. Traverse data for the advanced design turbine are presented in Figs. 58.36 and 58.37 for the last stationary blade inlet. Flow incidence is presented as a function of blade height for high and low values of specific mass flow. Good agreement is indicated between prediction and the traverse data. As flow rate (and load) decrease, the correspondence between test and calculation becomes less convincing, indicating that loss mechanisms existing under part-load operation are not as well defined as at high load near the design point.

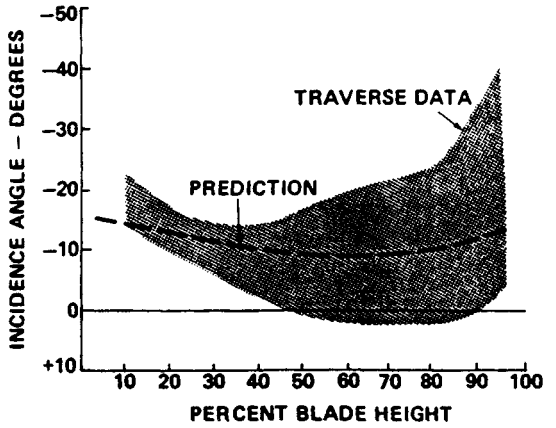

Fig. 58.36 Last stationary blade incidence angle at high-end loading—12,000 lb/hr-ft^2.

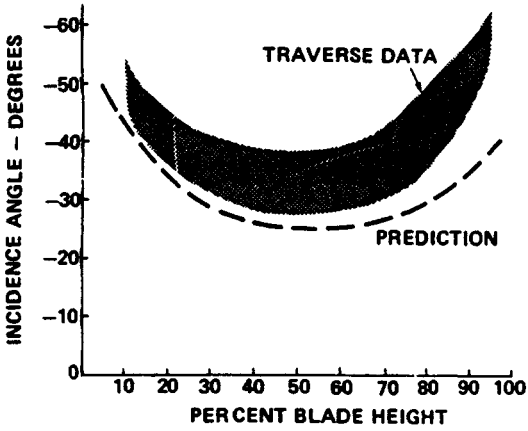

Fig. 58.37 Last stationary blade incidence angle at low end loading—6,000 lb/hr-ft^2.

By calculation, utilizing the rotor blade downstream traverse data, it is possible to determine the operating conditions relative to the rotor blade. That is, the conditions as seen by a traveler on the rotor blade can be determined. Figure 58.38 presents the Mach number leaving the last rotor blade (i.e., relative to it) as a function of blade height compared to the expected variation. Very high Mach numbers are experienced in this design and are a natural consequence of the high rotor blade tip speed, which approximates 2010 ft/sec, which converts to a wheel speed Mach number of 1.61.

In a manner similar to that applied at the inlet of the last stationary blade, the characteristics at the exit of this blade can be determined. Results of this traverse are shown in Fig. 58.39, where the effects of the stator wakes can be identified. The high Mach numbers experienced at the stationary blade hub make this particular measurement extremely difficult. The comparison shows good agreement, with expectations for this difficult measurement location.

The combination of these stationary blade exit traverses with velocity triangle calculations enables the flow conditions at the inlet of the rotor blade to be determined. Flow incidence as a function of blade height (diameter) is presented in Fig. 58.40 for the high-end load condition of Fig. 58.36. Significant flow losses can be incurred by off-design operation at high incidence levels. The hub and tip are particularly sensitive, and care must be taken in the design process to avoid this situation.

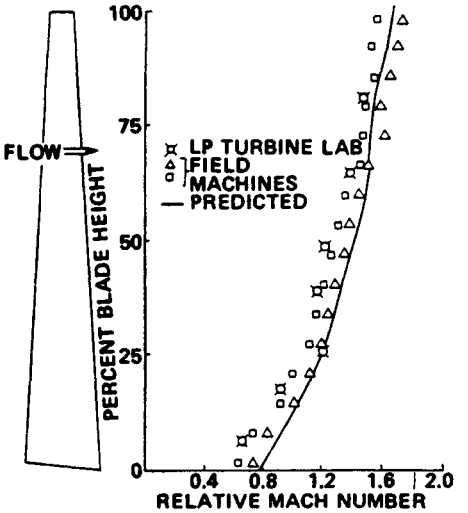

Fig. 58.38 Mach number relative to last rotating blade.

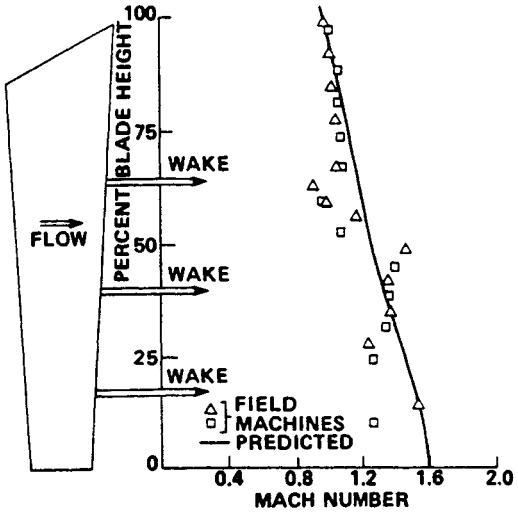

Fig. 58.39 Mach number at exit of last stationary blade.

Further confirmation of the design process can be achieved by evaluation of the kinetic energy leaving the last stage. This energy is lost to the turbine and represents a significant power output if it were possible to convert it to useful work. This kinetic energy, or *leaving loss,* is defined as

$$\overline{V}^2 = \int_{\text{Hub}}^{\text{Tip}} (\rho V) \frac{V^2\, dA}{\dot{M}} \tag{58.33}$$

and plotted in Fig. 58.41 as a function of exhaust volumetric flow. Excellent agreement has been achieved between the test data and prediction.

The foregoing represents conventional practice in the design of low-pressure blading as well as the design and analysis of upstream blading located in the HP and IP cylinders. The capability of solving the Navier–Stokes equations is now available. Drawbacks to this approach are the complexities of constructing a three-dimensional model of the subject of interest and the computational time required. The current philosophy regarding the use of Navier–Stokes solvers is that their practical application is to new design concept developments in order to determine valid and optimum resolutions of these concepts. In this process, design guidelines and cause-and-effect relationships are

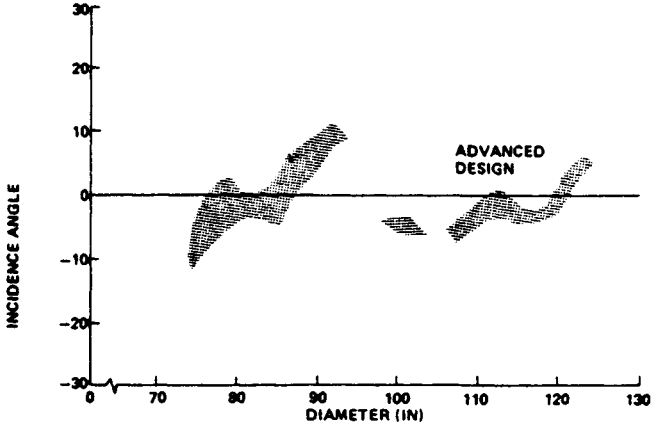

Fig. 58.40 Last rotating blade incidence angle at high-end loading.

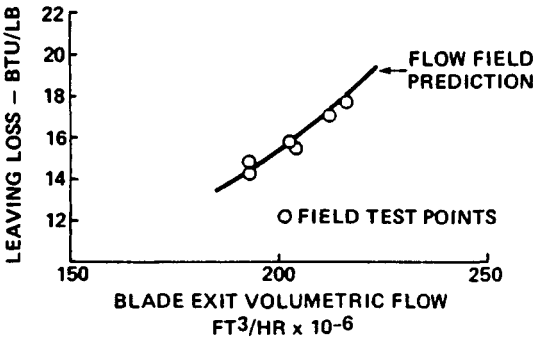

Fig. 58.41 Leaving loss as a function of exhaust volumetric flow for an advanced design.

developed for subsequent application to production machinery. As of this writing, their day-to-day use is prohibited by manpower and computer time requirements. Nevertheless, significant improvements in, and changes to, the conventional design process have been made by the Navier–Stokes solvers. For the steam turbine aerodynamicist, the most influential approaches are those developed by Denton,[11] a program *not* a Navier–Stokes solver but having three-dimensional inviscid capability, and that by Dawes,[12] a truly three-dimensional Navier–Stokes solver.

58.4.7 Blade-to-Blade Flow Analysis

The blade-to-blade flow field problem confronts the turbine designer with a variety of situations, some design, and some analysis of existing designs. The flow regime can vary from low subsonic (incompressible) to transonic with exit Mach numbers approaching 1.8. The questions to be resolved in blade design are what section will satisfy the flow field design, and how efficiently it will operate.

From the mechanical viewpoint, will the blade section, or combination of sections, be strong enough to withstand the steady forces required of it, centrifugal and steam loading, and will it be able to withstand the unknown unsteady forces impressed upon it? The structural strength of the blade can be readily evaluated as a function of its geometry, material characteristics, and steady stresses induced by steady loads. The response of the blade to unsteady forces, generally of an unknown nature, is a much more formidable problem. Tuning of the long, low pressure blade is a common occurrence, but as blades become shorter, in the high and intermediate pressure elements, and in the initial stages of the low-pressure element, tuning becomes a difficult task. Blades must be designed with sufficient strength, or margin, to withstand these unsteady loads and resonance conditions at high harmonics of running speed.

The aerodynamic design of the blade depends on its duty requirements, that is, what work is the blade expected to produce? The fluid turning is defined by the flow field design, which determines the radial distribution of inlet and exit angles. Inherent in the flow field design is the expectation of certain levels of efficiency (or losses) that have defined the angles themselves. The detailed blade design must then be accomplished in such a manner as to satisfy, or better, these design expectations. Losses then, are a fundamental concern to the blade designer.

54.4.8 Blade Aerodynamic Considerations

Losses in blade sections, and blade rows, are a prime concern to the manufacturer and are usually considered proprietary information, as these control and establish its product's performance level in the market place. These data and correlative information provide the basic guidelines affecting the design and application of turbine–generator units.

Techniques involved in identifying and analyzing blade sections are more fundamentally scientific and have been the subject of development and refinement for many years. Current processes utilize the digital computer and depend on numerical techniques for their solution.

Early developments in the analysis of blade-to-blade flow fields[13] utilized analogies existing between fluid flow fields and electrical fields. A specific application can be found in Ref. 11.

Transonic Blade Flow

The most difficult problem has been the solution of the transonic flow field in the passageway between two blades. The governing differential equations change from the elliptic type in the subsonic flow regime to the hyperbolic type in the supersonic regime, making a uniform approach to the problem solution mathematically quite difficult. In lieu of, and also in support of, analytic procedures to define the flow conditions within a transonic passage, experimental data have been heavily relied upon. These test programs also define the blade section losses, which is invaluable information in itself.

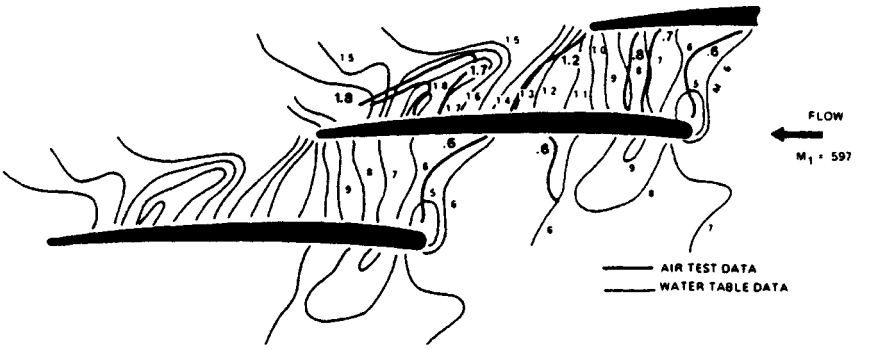

Fig. 58.42 Comparison of water table test results with interferometry air test data for Mach number distribution in transonic blade.

Testing and evaluating blade section performance is an art (and a science) unto itself. Of the several approaches to this type of testing, the air cascade is by far the most common and manageable. Pressure distributions (and hence Mach number) can be determined as a function of operating conditions such as inlet flow direction (incidence), Reynolds number, and overall pressure ratio. Losses also are determinable. Optical techniques are also useful in the evaluation of flow in transonic passages. Constant density parameters from interferometric photos can be translated into pressure and Mach number distributions.

A less common testing technique is the use of a free surface water table wherein local water depths are measured and converted to local Mach number.[14] The analogy between the water table and gas flow is valid for a gas with a ratio of specific heats equal to 2, an approximation, to be sure. A direct comparison of test results for the same blade cascade is presented in Fig. 58.42. The air test data were taken from interferometric photos and converted to parameters of constant Mach number shown in heavy solid lines. Superimposed on this figure are test data from a free-surface water table in lighter lines. A very good comparison is noted for these two sets of data from two completely different blade-testing concepts. The air test is more useful in that the section losses can be determined at the same time the optical studies are being done. The water table, however, produces reasonable results, comparable to the air cascade as far as blade surface distributions are concerned, and is an inexpensive and rapid means of obtaining good qualitative information and, with sufficient care in the experiment, good quantitative data.

Analytical Techniques

Various analytic means have been employed for the determination of the velocity and pressure distributions in transonic blade passages. A particular technique, termed *time marching,* solves the

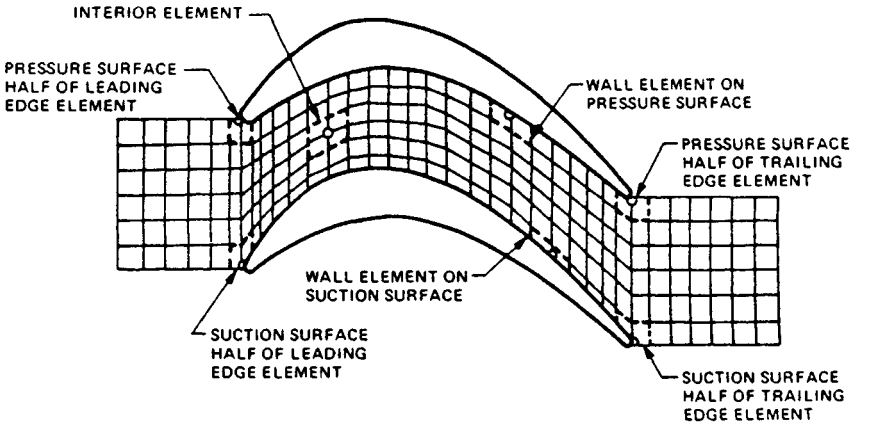

Fig. 58.43 Blade-to-blade calculational region.

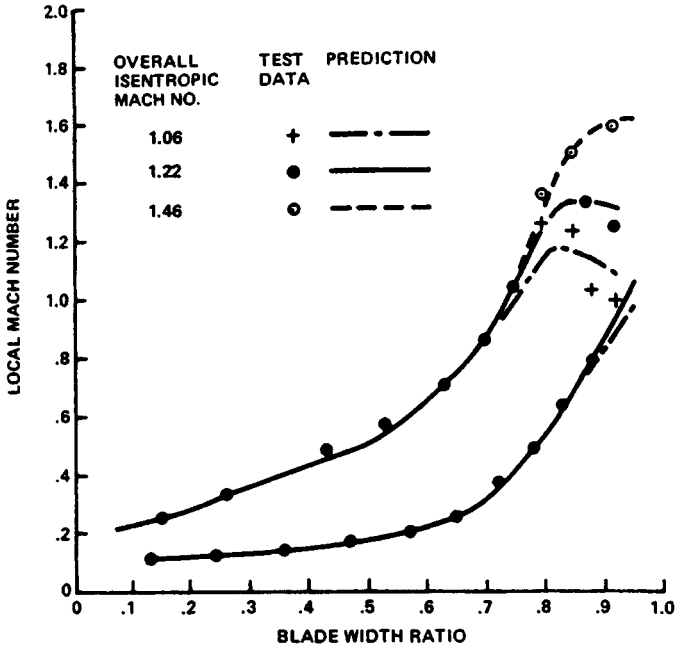

Fig. 58.44 Local Mach number distribution on transonic blade surfaces.

unsteady compressible flow equations by means of successive calculations in time utilizing a flow field comprised of finite area, or volume, elements. Figure 58.43 presents the general calculation region describing the flow passage between two blades. A result of the time marching method is shown in Fig. 58.44, which presents a plot of local Mach number along both the suction and pressure sides of a transonic blade. Parameters of exit isentropic Mach number show a significant variation in local surface conditions as the blade's overall total to static pressure ratio is varied. These data were obtained in air from a transonic cascade facility. In summary, sophisticated numerical processes are available and in common use for the determination of blade surface pressure and velocity distributions. These predictions have been verified by experimental programs.

REFERENCES

1. A. I. Kalina, "Recent Improvements in Kalina Cycles: Rationale and Methodology," *American Power Conf.* **55** (1993).
2. ASME, *The 1967 ASME Steam Tables,* ASME, New York.
3. W. G. Steltz, "The Critical and Two Phase Flow of Steam," *J. Engrg. for Power* **83**, Series A, No. 2 (1961).
4. Babcock and Wilcox, *Steam, Its Generation and Use,* Babcock and Wilcox, 1992.
5. Westinghouse, *Westinghouse Steam Charts,* Westinghouse Electric Co., 1969.
6. H. R. M. Craig and H. J. A. Cox, "Performance Estimation of Axial Flow Turbines," *Proc. Inst. of Mech. Engs.* **185**(32/71) (1970–1971).
7. S. C. Kacker and U. Okapuu, "A Mean Line Prediction Method for Axial Flow Turbine Efficiency," *J. Eng. for Power* **104**, 111–119 (1982).
8. M. J. Moore and C. H. Sieverding, *Two Phase Steam Flow in Turbines and Separators,* McGraw-Hill, New York, 1976.
9. C. H. Wu, "A General Theory of Three-Dimensional Flow in Subsonic and Supersonic Turbomachines of Axial-, Radial-, and Mixed-Flow Types," NASA TN 2604, 1952.
10. W. G. Steltz, D. D. Rosard, P. H. Maedel, Jr., and R. L. Bannister, "Large Scale Testing for Improved Reliability," American Power Conference, 1977.
11. J. D. Denton, "The Calculation of Three-Dimensional Viscous Flow Through Multistage Turbines," *J. of Turbomachinery* **114** (1992).
12. W. N. Dawes, "Toward Improved Throughflow Capability: The Use of Three-Dimensional Viscous Flow Solvers in a Multistage Environment," *J. of Turbomachinery* **114** (1992).

13. R. P. Benedict and C. A. Meyer, "Electrolytic Tank Analog for Studying Fluid Flow Fields within Turbomachinery," ASME Paper 57-A-120, 1957.

14. R. P. Benedict, "Analog Simulation," *Electro-Technology* (December 1963).